Aeolian sediment transport on a beach

Testing the AeoLiS aeolian sediment transport model against the observed recovery of Fire Island

MSc Thesis Tom Janssen

Delft University of Technology
Faculty of Civil Engineering and Geosciences
Department of Hydraulic Engineering

August 2016

Report type
MSc. Thesis Delft University of Technology

Title
Aeolian transport on a beach

Subtitle
Testing the AeoLiS aeolian sediment transport model against the observed recovery of Fire Island

Date
August 5th 2016 – Final draft

Author

Name:	Tom Janssen
Student no:	4008898
University:	Delft University of Technology (DUT)
Faculty:	Civil Engineering and Geosciences
Program/track:	Hydraulic Engineering, Master of Science Civil Engineering
Specialization:	Coastal Engineering

Graduation Committee

Chairman	prof. dr. ir. A.J.H.M. Reniers	*Fluid Mechanics, DUT*
First supervisor	ir. A.R. van Dongeren, Ph.D.	*Applied Morphodynamics, Deltares*
Supervisor	ir. B.M. Hoonhout	*Coastal Engineering, DUT and Deltares*
Supervisor	ir. J.P. den Bieman	*Coastal structures and Waves, Deltares*
Supervisor	dr. N.G. Plant	*St. Petersburg Coastal and Marine Science Center, USGS*
Supervisor	dr. ir. S. de Vries	*Coastal Engineering, DUT*

In collaboration with

Deltares

U.S. Geological Survey

Credits photo cover page: Owen Brenner, USGS

ABSTRACT

Fire Island has been monitored since Hurricane Sandy (2012). During that period, Fire Island showed recovery (accretion on the island). Behaviour of the recovery is not yet well-known. Main processes during the recovery are also not known. Therefore, the emphasis of this thesis is on the understanding of the main processes of the recovery of barrier islands, with Fire Island, New York, United States as a case study.

AeoLiS has been validated for the Sand Motor, Kijkduin in The Netherlands. From this study it is (1) not known whether AeoLiS would have the same predictive skill at other locations and (2) not clear what parameters at a new site would affect skill and model sensitivity the most. Fire Island differs from the Sand Motor as the beach width of Fire Island is significantly smaller. Therefore, the focus of this thesis is on the beach width and its effect on the aeolian sediment supply and transport. Testing the model at a new location will also indicate what additional data or processes are missing in the present AeoLiS model which are required to perform a hindcast.

The main processes and behaviour in the recovery of Fire Island are analysed in a data analysis. The results of the analysis showed that, during the period 7 November 2012 until 26 September 2013, there was an accretion of the dunes. In this period the island was recovering from the impact of Hurricane Sandy. During this accretion period a welding bar was observed. This welding bar could be an important mechanism for the dune accretion growth as accretion was seen in the period after the welding of the bar. The reason for this accretion could be the increasing fetch and the addition of new sediment. Under idealized circumstances it can be assumed that the total flux settles in the dunes. The determination of the total transport under these circumstances using Bagnold's formulation indicates a larger increase than is actually measured. This indicates that the actual accretion of the dunes is limited.

The AeoLiS model was used to hindcast the recovery of Fire Island, during the period 7 November 2012 until 26 September 2013, by predicting the transport rate into the dunes. It is assumed that the total flux into the dunes will settle in the dunes. Comparing these results to the data analysis, showed that the hindcast was in the same range. The general validity of the results depends on several assumptions. The main assumption is; the model only included onshore transport, while the wind direction was variable and mainly offshore during the accretion period. The sensitivity analyses indicated that the model simulation of Fire Island is most sensitive for a variation in the beach width and the median grain size. Furthermore, it can be concluded that aeolian sediment transport on Fire Island is often transport limited (85%) but occasionally supply limited (15%).

From this research it can be concluded that there are processes and data missing for a hindcast with the AeoLiS model. The improvements for the AeoLiS model can be summarized as improvements to the initial conditions, as follows:

1. The accretion of Fire Island in the data analysis is based on lidar data. The lidar data is compared to 1D transects. Those 1D transects are also imposed in the AeoLiS model. Using a 2DH bathymetry with both x-directions and y-directions could give more information about aeolian sediment transport.
2. The grain size distribution for Fire Island is not known in detail. The sensitivity analysis indicated that the effect of the uncertainty of the mean and standard deviation of the grain size distribution on the total transport is 13%.

ACKNOWLEDGEMENTS

This thesis is written as the final chapter of the Master of Science program Hydraulic Engineering at the Faculty of Civil Engineering and Geosciences at the Delft University of Technology. The research for this thesis has been hosted and facilitated by Deltares in Delft, the Netherlands, and USGS Coastal and Marine Science Center in Saints Petersburg, Florida, United States of America.

First of all, I am grateful to my supervisors at Deltares: Ap van Dongeren, for introducing me to the topic and hosting the research, Bas Hoonhout and Joost Den Bieman, for helping and advising me with daily problems, but also for your feedback and critical minds that contributed to better results and representation of this thesis. Furthermore, I want to thank my graduation committee members Ad Reniers and Sierd de Vries for the valuable discussions and insights.

Special thanks go to Nathaniel Plant for being part of my graduation committee, but even more for hosting part of my research in Saint Petersburg. I really appreciated the hospitality and your help with everything during my stay from the data analysis but also fixing a flat tire. Therefore, I also want to thank Kathleen Wilson, Owen Brenner and Jennifer Miselis for helping me finding my way in data and knowledge at the USGS.

I also would like to thank my colleague graduation students at Deltares and Laurens Poelhekke in particular for introducing me to Deltares and Ap van Dongeren. I would like to close by thanking my family and friends from 'de Pret', 'de Mola', 'Styx' and 'Het Waterbouwdispuut' for all your support during my graduation!

Tom Janssen

Delft, July 2016

CONTENTS

1 INTRODUCTION

1.1 BACKGROUND

Coastal zones are among the most populated places around the world and are the places where the most economic activity takes place (Nganyi et al., 2010). The importance of protecting people and infrastructure against flooding from the sea becomes increasingly essential, because future coastal hazards can have significant impacts in those areas. Therefore, it is necessary to know how human interventions or natural processes affect coastal safety. There are several elements that can protect a coastal zone. One of these elements, which is primarily natural, is a barrier island. Barrier islands shelter the mainland coast behind it from wave attack and surges (Bosboom & Stive, 2013). These islands, for example, are a prominent feature of the US Atlantic and Gulf of Mexico coastlines from New York to Texas. The Wadden Islands stretching from the Netherlands through Germany to the west of Denmark are another example.

An understanding of the combination of storm induced erosion and the recovery in between storm events is required to predict the long-term morphological behaviour of barrier islands. During recovery the coast is preparing to withstand a subsequent storm. In the framework of the United States Geological Survey (USGS) cooperation the barrier island Fire Island, New York, USA is chosen as case study site to research the recovery of a barrier island. The USGS is monitoring the recovery of Fire Island, following severe impacts to the barrier island during Hurricane Sandy (2012). The on-going Fire Island Coastal Change research is primarily focused on understanding the short-term (seasonal to annual) and long-term (decadal to centennial) behaviour of the Fire Island barrier island system.

Fire Island is centrally located in the outer barrier island system parallel to the south shore of Long Island, New York (Figure 1). From Fire Island Inlet in the west it is approximately 50 kilometres to Moriches Inlet in the east (Figure 6). There are seventeen communities interspersed between National Park lands with only few hundred people living year round on the island. However, during the summer months, this population will increase to a few thousand. The island also contains the Otis Pike High Dune Wilderness and two state parks (USGS, 2016).

Figure 1; Overview Fire Island, US (source: Google Earth/Wikipedia)

Models can help with the interpretation of the recovery of Fire Island. At this moment assessment models typically consider erosion (long-term or storm-induced) but not the recovery between storms (e.g. XBeach,

Roelvink et al., 2009). The development of barrier islands in the recovery period between storm events is still not well understood. Therefore, the recovery period in between storm events is especially interesting. Consequently, models cannot be applied accurately over longer periods from a starting bathymetry. It is important to notice that storm events occur on a different timescale than the recovery in between storm events. For example, storm events will at most take a couple of days and have an interval of months, years or decades, while the recovery could take a couple of weeks to months or even years.

AeoLiS is a process-based aeolian sediment transport model intended to simulate dune growth and recovery. The model is validated for the Sand Motor mega nourishment (Stive et al., 2013), but still requires validation for more common coastal environments, including barrier islands. AeoLiS can help with the interpretation of the recovery of Fire Island.

In this thesis, the emphasis is on the processes around the waterline during recovery periods. For the recovery of a barrier island, sediment from the sea is required. Dune development is dependent on the landward migration and welding of nearshore bars and, therefore, the focus in this thesis is on the phenomenon of welding bars to provide the required sediment (Houser, 2009). During the monitoring program on Fire Island, the landward migration and welding of bars have been observed.

1.2 PROBLEM DEFINITION

Fire Island has been monitored since Hurricane Sandy (2012). During this period, Fire Island showed recovery (accretion on the island). Behaviour of the recovery is not yet well-known. Main processes during the recovery are not known as well. Therefore, the emphasis of this thesis is on the understanding the main processes of the recovery of barrier islands, with Fire Island as a case study.

AeoLiS has been validated for the Sand Motor. From this study it is (1) not known whether AeoLiS would have the same predictive skill at other locations and (2) not clear what parameters at a new site would affect skill and model sensitivity the most. Fire Island differs from the Sand Motor in that the beach width of Fire Island is significantly smaller. Therefore, the focus in this thesis is on the beach width and its effect on the aeolian sediment supply and transport. Bar welding can affect the beach width and is, therefore, a feature of interest. Testing the model at a new location can also indicate what additional data or processes are missing in the present AeoLiS model to be able to perform a hindcast.

1.3 RESEARCH OBJECTIVES

The research questions are:

1. What are the main processes and behaviour in the recovery of Fire Island?
2. Is the AeoLiS model able to hindcast the recovery of Fire Island?
3. What processes and data are missing for a hindcast with the AeoLiS model?

1.4 METHODOLOGY

To answer the above mentioned research questions, a research method has been created. It is important to initially understand the model and behaviour of parameters before making it more complex. Therefore the research is separated in several studies.

Literature study: focus is on the processes related to the recovery of Fire Island. Furthermore, the AeoLiS model is studied by literature and application to conceptual cases.

Data analysis: the Fire Island Coastal Change research is investigated to understand main processes and behaviour in the recovery of Fire Island.

Hindcast study: the AeoLiS model is tested for its ability to hindcast the recovery of Fire Island. A sensitivity analysis helps in better understanding important processes. Furthermore, lacking processes can be identified.

1.5 READING GUIDE

This report is organized following the research process. In Chapter 1 the problem definition and their research objectives are stated. In the literature study, Chapter 2, background information on the coastal zone, sediment transport, storm recovery and welding bars are provided. Chapter 2 gives also a description of the AeoLiS model and the adjustments made for this research. The data availability and analysis done on Fire Island is elaborated on in Chapter 3. Both gathering of data and analysis of data is discussed. Chapter 4 shows the results of one cross-shore profile, result of other profiles are provided in the appendices. The conceptual model results and model results based on Fire Island conditions are presented and explained in Chapter 4. Subsequently, in Chapter 5 the results of both the data analysis and the model are discussed. Finally, conclusions are drawn and recommendations are given in Chapter 6.

2 LITERATURE STUDY

In this chapter, background information and the explanation of general physics is given concerning some key aspects relevant to the proposed research.

2.1 COASTAL ZONE

2.1.1 INTRODUCTION

In this thesis, definitions of the coastal zone stated by the U.S. Army Corps of Engineers are used (cited by den Bieman, 2012) as shown in Figure 2. The back barrier (bay) with, optionally, a beach is specifically for a barrier island. A coastal zone has dunes and a coastal hinterland landwards from the foredune.

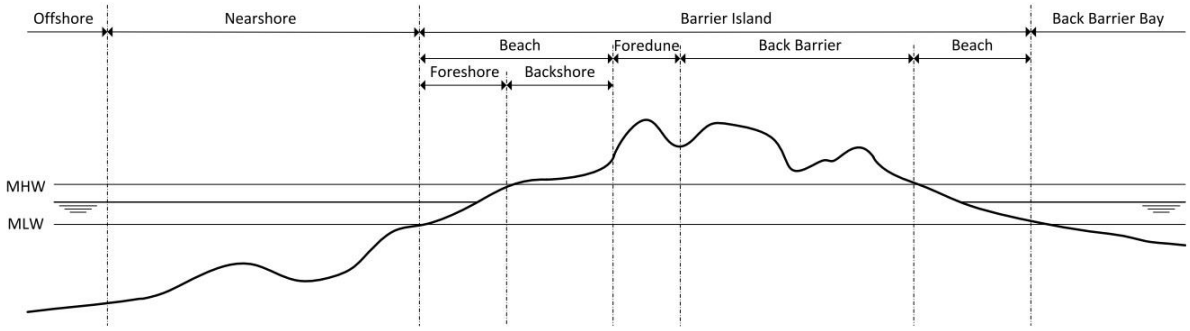

Figure 2: Definitions used to describe features in the coastal zone (den Bieman, 2012)

The offshore zone starts at water depths of approximately 20 m, typically the limit of the morphologically active zone. The nearshore is the part of the profile located from a water depth of 20 m and seaward of the mean low water (MLW) line. The nearshore is affected by wave action and the place where breaker bars are found. The zone between the MLW line and the mean high water (MHW) line is known as the foreshore. The backshore extends from MHW until the dune foot. The foredune is the most seaward dune and is followed by different features such as other dunes, dune ponds, supratidal marshes, vegetated barrier flats and washover fans. This zone is known as the back barrier. The back barrier bay is the bay located landward of the barrier island. This bay is connected to the sea by tidal inlets. The character of the bay can be submerged or contain intertidal salt marshes with tidal creeks.

2.1.2 BARRIER ISLANDS

Barrier islands are frequent recognized offshore features which protect the mainland and enclosed lagoons from direct wave attack by the sea. These islands, for example, are a prominent feature of the US Atlantic and Gulf of Mexico coastlines from New York to Texas. The Wadden Islands stretching from the Netherlands through Germany to the west of Denmark are another example. Consequently, many different types of islands exist and in many ways each island is unique. Barrier islands exhibit a wide range in size and overall shape. This diversity stems from large variations in sediment supply, tidal range, and wave energy.

Leatherman (1982) divided the barrier island into four main classes by distinguishing the tidal range and the sediment supply. The tidal range was divided into two groups: microtidal (tidal range smaller than 1.8m) and mesotidal (tidal range of 1.8-3.6m). A larger tidal range could exist but is unusual for a barrier island and is, therefore, disregarded. The barrier islands are also divided into barrier islands with sediment deficiency (transgressive, potential for erosion) and barrier islands that have a history of accretion (regressive). The four

main classes are shown in Table 1. Fire Island can be described as a microtidal transgressive barrier island. Therefore, Fire Island is vulnerable to storms and resides in the least stable barrier islands class. Chapter 3 is a more extensive analysis of Fire Islands' coastal zone.

Table 1; Barrier Island classes by Leatherman **(1982)**

Barrier island classes (Leatherman 1982)	Description
Microtidal transgressive barrier islands	Long and narrow islands with low topography, least stable barrier island class and most vulnerable to storms. Washovers indicate deficiency of sediment and retreat of the shoreline.
Microtidal regressive barrier islands	Also washovers as a result of storms. Stability of the island is indicated by the amount of dune ridges, more ridges more stability.
Mesotidal transgressive barrier islands	Short in length compared to the width of the island. Inlets in between barrier islands are more stable than for mictrotidal barrier islands because of the daily exchange of a larger amount of water from the ocean to the bay.
Mesotidal regressive barrier islands	Drumstick shape of the island, middle of the island is the most stable with dune ridges. The updrift and downdrift end can be subject to erosional and accretionary trends.

2.1.3 FIRE ISLAND, NEW YORK, UNITED STATES OF AMERICA

The barrier island of Fire Island has been subject to several researches. These researches can help in better understand the results of the data analysis described in Chapter 3.

Leatherman (1985) investigated the morphological changes around Fire Island based on data concerning the last 150 years. The author divided the island in different transects to analyse them separately and investigate differences. The geomorphic and stratigraphic (studies on rock layers and layering) analysis led to 6 conclusions:

1. There are differences for the east and west part of the island. These differences appeared to be related to relative barrier stability and to the rate of landward barrier migration due to physiographic features (physical patterns and processes to produce and change parts of the earth) and vegetation.
2. Overwash events did not result in sediment transport to the back barrier bay, so it contributed to the island migration
3. Processes at the inlet caused sediment transport to the back barrier bay and therefore landward barrier migration
4. Western Fire Island has experienced shore face erosion and back barrier beach erosion and submergence over the past 1000 years.
5. Eastern Fire Island appeared to have been more dynamic and to have experienced a more rapid rate of migration than western Fire Island
6. The trend of long-term landward barrier migration, common to other barrier island at the US east coast is also applicable for Fire Island.

Hapke et al. (2010) did sediment budget analyses for the Fire Island coast. Alongshore components (east to west) are well known rather than cross-shore components. The authors found a yearly average deficit of sediment. This indicated that an onshore component of sediment transport is likely more important along Fire Island than previously thought. So, nearshore Holocene sedimentary deposit is possible transported to the shoreline (Schwab et al., 2013).

2.2 SEDIMENT TRANSPORT PROCESSES

When investigating morphological change, it is helpful to understand the hydrodynamic and aeolian physical processes inducing sediment transport. In this research, emphasis is on a 1D analysis of the barrier island processes. So, the focus is on the cross-shore dimension and, therefore, the alongshore sediment transport processes will not be treated. The emphasis in this research is on the recovery of the barrier island and, especially, the role of aeolian sediment transport. Sediment transport is divided in aeolian and hydrodynamic transport. Therefore to minimize complexity, morphological change as result of hydrodynamic transport is imposed, because morphologic changes are not included in the AeoLiS model.

Aeolian transport can be divided in suspended and bed-load transport. The bed-load transport can be further divided into saltation and rolling or sliding (reptation). When typical sand storms are considered (first research in aeolian transport was in a desert environment) particles with a maximum diameter between 40 and 60 µm can be transported in suspension. The sand in coastal sediment has a typical diameter ranging from 100 to 500 µm and is therefore transported primarily via bed-load. Therefore, the suspension load can often be neglected. Saltation and reptation will not be further distinguished, because both contribute in the total bed load transport (Sauermann et al., 2001).

To start saltation transport, some grains in the bed have to be entrained by the wind. Those grains have a certain flight time before they hit the bed again because of drag forces. When a grain hits the bed again, it transfers momentum to the grains in the bed. The wind can entrain those grains again (Figure 3). Chapter 2.3 describes in more detail aeolian sediment.

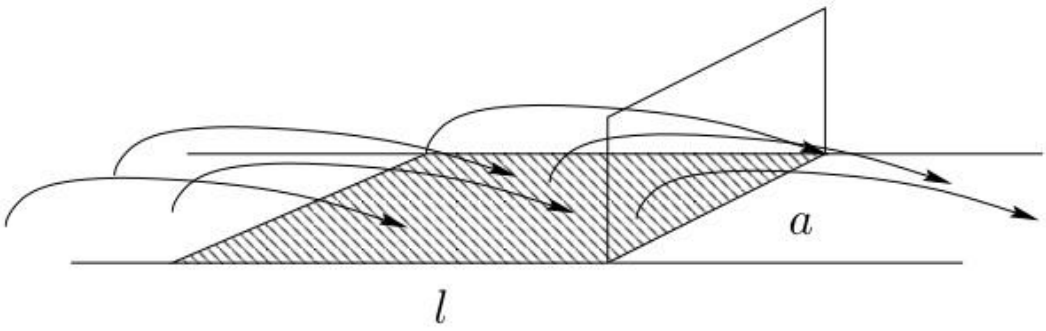

Figure 3: Principle of saltation, the arrows present the saltating grains , *l* = mean trajectory length, *a* = arbitrary width (Sauermann et al., 2001)

2.2.1 STORM RECOVERY

Compared to studies that document beach and dune erosion during storms, the post storm recovery has received less attention in literature. Houser & Hamilton (2009) found that the alongshore variation in recovery depends on transverse ridges on the inner shelf, the height of the pre-storm dunes, the amount of overwash penetration and the presence of vegetation. Therefore, the recovery does not solely depend on the width of the island. The presence of vegetation allows for a greater dune recovery compared to dunes without vegetation. The sections of an island where vegetation is not able to return in time are more vulnerable than those with historically limited dune development. Houser et al. (2015) found that the recovery of the beach and dune to pre-storm morphology could take up to a decade. The amount of recovery is dependent on the pre-storm dune height. Thus, larger dunes take longer to recover.

The importance of vegetation is also indicated by Duran & Moore (2013). The authors argue that vegetation controls coastal vulnerability to storms by determining maximum dune size rather than sediment supply. Vegetation increases also the capability of withstanding dune destabilization. The authors extend the Dune model introduced by Kroy et al. (2002) based on aeolian transport processes (Section 2.2; Sauermann et al., 2001) to included ecological and physical effects of a coastal environment. The Coastal Dune Model quantifies the foredune development that is affected by wind, sediment transport, topography, the shoreline and vegetation.

De Vries et al. (2012) made a first step to fulfil the goals. The authors found that the dune volume changes in the Netherlands are often linear in time. No significant correlation is found between the variability of yearly wind conditions and yearly dune volume changes. The authors concluded that in future modelling of yearly to decadal dune volume changes, variability such as supply limiting parameters is of interest rather than time varying forcing conditions such as varying wind velocities and drift potentials.

Houser (2009) stated that, after dune erosion, dune recovery requires recovery of the beach through the onshore migration and welding of nearshore bars (section 2.2.3) followed by accretion in the backshore to create a supply of sediment for transport by wind. The problem is that existing beach-dune models do not consider how and when sediment gets transferred to the backshore and, where it becomes available for transport by the wind. Also in the research on the influence of high water levels on aeolian transport done by Ruz & Meur-Ferec (2004), they concluded that an interaction with the intertidal area is required to predict the behaviour of the upper and therefore the dune evolution on a microtidal coast. A combined analysis of changes in beach volume, meteorological data and water levels prevailing during the survey period are required. So, a feature in the intertidal area could be the source for the dune evolution.

2.2.2 BEACH WIDTH

Fire Island differs from the Sand Motor in that the beach width of Fire Island is significantly smaller. Therefore, the focus in this section is effect of beach width on aeolian sediment transport.

Bauer & Davidson-Arnott (2003) investigated the equilibrium sediment transport load. The maximum transport is affected by the width of the beach. The beach width where equilibrium occurs is called the critical fetch distance. If the beach width is smaller than the critical fetch no equilibrium is reached. If the fetch on the beach is larger than the critical fetch distance there will be an equilibrium sediment transport. The fetch can occur under an angle on the beach. Thus, the critical fetch can be used to predict total potential sediment losses from the beach system due to aeolian action, as well as to simulate the potential evolution of a coastal dune field. The critical fetch distance is not a constant parameter but depends on beach parameters such as geometry, moisture content and wind direction (Delgado-Fernandez, 2010). Therefore, the critical fetch distance is not practical to use, but it gives a better understanding of the effect of the beach width on the transport processes.

Bauer et al (2009) did not only look into the fetch. The authors identify more important factors concerning the aeolian sediment transport across beaches such as the interaction between the beach geometry, surface conditions and wind field attributes. The transport potential is reduced by substantial moisture content in the surface sediments. Moisture conditions are time dependent, tides and waves influence the fore shore, whereas the rest of the beach and dunes is influenced by the atmospheric humidity, precipitation events and possibly groundwater. The authors also state the importance of the influence of waves on the variation of the beach geometry. The same holds for the varying wind affects the equilibrium aeolian sediment transport as mentioned before. The challenge identified by the authors is to generate a better understanding of the factors that influence sediment transport flux as a function of downwind distance across a beach.

2.2.3 WELDING BARS

A feature in the intertidal area could be the source for the dune evolution. It was hypothesized that welding bars could be a feature that affects the dune evolution. A bar is a submerged embankment of sediment that is located parallel to the shore. Bars are the result of breaking waves and cross-shore currents. Bars are very mobile and there could be multiple bars cross-shore (Bosboom & Stive, 2013). Lippmann et al. (1993) investigated the near shore bar system for five years in Duck, North Carolina, USA, a coast 500 kilometres south of Fire Island. The near shore bar system at Duck consisted mainly out of two bars cross-shore.

Walstra et al. (2012) described four types of bar response; onshore or offshore migration of a bar with a bar amplitude increase or decrease. This behaviour depends on the water depth above the bar crest and the angle of wave incidence. Those parameters can give more information on wave breaking on the bar and an alongshore current. In general, bars originate nearshore and mitigate offshore to the end of the surf zone. For example in Noordwijk, the Netherlands, a cycle of bar mitigation every three years is found.

Onshore bar migration was the subject of a two day spanning field survey of Aagaard et al (2006). The onshore migration of the bar was caused by a runnel on the beach. Sediment transport was directed onshore and after passing the crest of the bar the water flowed alongshore in the runnel. The bar migrated at a rate of 10-20 meters per day. When the bar filled the runnel with sediment, offshore sediment transport started by an undertow. This caused the disappearing of the bar again. This is an example to show how a welding bar acts in reality and ratifies the concept of a welding bar. At the Fire Island coast, welding bars are observed but not studied as detailed in time as this research. This research could demonstrate the process of bar welding at Fire Island.

Houser et al. (2006) researched the behaviour of an intertidal swash bar. The authors found a relation between the breaker zone and the migration direction of a swash bar. The swash bar migrates onshore when the breaker zone is on the seaward slope of the bar and is offshore directed when the breaker zone is on bar crest. The results were based on seven storm events; during the storm events the breaker zone was affected by the water level, local wave heights and the bathymetry at the time of the storm.

From those papers can be concluded that swash bars can lead to foreshore accretion. So, when a swash bar migrates onshore and the sediment is above water level the sediment of the bar can be the source for aeolian sediment transport. Therefore a welding bar could be followed by accretion backshore (dune accretion) as a result of aeolian sediment transport (Houser, 2009). The bar welding can also increase the width of the beach. These hypotheses are tested in the data analysis (Chapter 3) and the model study (Chapter 4).

2.3 THE AEOLIS MODEL

2.3.1 INTRODUCTION

Current models are based on Bagnold (1935) and alternatives such as Hsu (1971), Owen (1964) and Kawamura (1951) that determine aeolian sediment transport rate (q in kg/m/s) depending on shear velocity (threshold) (u_* and u_{*th} in m/s) and a collection of parameterizations (A):

$$q = A \cdot \left(u_* - u_{*th}\right)^3 \quad (1)$$

De Vries et al. (2014) described a model approach for aeolian sediment transport in supply limited situations. Compared to current sediment transport models, the approach introduces a new variable to include sediment supply in the model.

Consequently, the transport rate is not solely dependent on the wind velocity, but also on the sediment availability. Moreover, due to the support of an advection formulation, transport can also vary spatially.

Hoonhout & de Vries (2016) continued previous research, extended the model approach by computing the spatiotemporal varying sediment supply through simulation and introduced the process-based AeoLiS model, a model for simulating coastal aeolian sediment supply and transport. The aeolian sediment transport in this model is not only dependent on wind but also on the sediment supply. The sediment availability can vary in time and space. Sediment sorting and armouring of the bed cause variations in sediment availability. A fully armoured bed is a top layer of the bed that only consists of material that is too large to be picked up by the wind. Under that top layer there can be finer grains available that can be picked up by the wind, but the armour layer of coarse material will prevent entrainment. There are intermediate forms of armouring where there are still grains in the bed that can be picked up by the wind. The spatiotemporal variations in the available sediment in the bed of the profile can have a significant effect on the long term aeolian sediment transport.

2.3.2 MODEL DESCRIPTION

In this section the important components of the model are discussed in more detail. In the model, grains from the bed are entrained by wind. Conditions for entrainment are that the wind velocity satisfies a threshold velocity and that there is sediment available. For a relatively large grain this threshold velocity will be larger than for a relatively small grain (Bagnold, 1935).

AeoLiS makes use of an 1D advection scheme in correspondence with De Vries et al. (2014):

$$\frac{\partial hC_t}{\partial t} + \frac{\partial u_* hC_t}{\partial x} = E - D \quad (2)$$

The 1D advection scheme determines the net entrainment (erosion (E) minus deposition (D) in kg/m^2). Further t (s) represents time and x (m) represents the cross-shore distance from a zero transport boundary (water line). The bed is discretized in horizontal grid cells. h (m) is the saltation height and C_t is the instantaneous sediment concentration (kg/m^3). The determination of the net entrainment is also based on De Vries et al. (2014):

$$E - D = \min\left(\frac{\partial S_e}{\partial t}; h \cdot \frac{C_u - C_t}{T} \right) \quad (3)$$

The net entrainment (E-D) is maximized by the available sediment in the bed (S_e) over time (t) and by the balance between the saltation height (h) multiplied by the equilibrium sediment concentration (C_u) and the instantaneous sediment concentration (C_t). T describes the adaptation time scale for both erosion and deposition. The adaptation time scale represents the time the instantaneous sediment concentration needs to adapt to the equilibrium sediment concentration. Variation of the wind velocity affects the equilibrium sediment concentration. In case more time is required to adapt, there is also more space required. So, the adaptation time scale and the critical fetch are related. If there is not enough space available to adapt, the beach width is too small, the transport is fetch limited. By default, the adaptation time scale is set to 1 second (de Vries et al., 2014).

The equilibrium sediment concentration is determined using an equilibrium sediment transport formulation (1) divided by the wind velocity (u_w). The mass per unit area ($\hat{C}$) is computed because the saltation height (h) is not solved.

$$hC_u = C_u = \max\left(0; \alpha C_b \frac{\rho_a}{g}\sqrt{\frac{d_n}{D_n}}\frac{(u_w - u_{th})^3}{u_w}\right) \quad (4)$$

α (-) is a constant to convert from measured wind velocity to shear velocity, C_b (-) is an empirical constant, ρ_a (kg/m^3) is the air density, g (m/s^2) is the gravitational constant, d_n (m) is the nominal grain size and D_n (m) is a reference grain size. Spatial variations in wind velocities and morphologic feedback are at this moment not included in the model. The focus is on sediment fluxes from the beach into the dunes and not on dune formations. α (-) is determined in equation (5) by the height of the measured wind velocity (z in metres) and the bed roughness (k in metres):

$$\alpha = \frac{0.174}{\log 10\left(\frac{z}{k}\right)} \quad (5)$$

The threshold velocity is determined in (6) by a constant in formulation for wind velocity threshold based on grain size (A (-)), the density of the grains and the air (ρ_p and ρ_a in kg/m^3), the gravitational constant and the nominal grainsize:

$$u_{th} = A \cdot \sqrt{\frac{\rho_p - \rho_a}{\rho_a} \cdot g \cdot d_n} \quad (6)$$

There are two limitations for the entrainment. The first limitation is the supply limitation. When there are no grains entrained by the wind, the aeolian sediment transport is limited or there is no wind. It is possible that there are still coarser grains available in the bed, but for those grains the threshold velocity is not satisfied. So for entrainment, there have to be grains available that meet the threshold velocity. So in a supply limited situation, the entrainment is less than it potentially could be by a lack of grains with a threshold velocity that is met. Therefore, in a supply limited situation, the sediment availability is smaller than there actually could be eroded for a given wind velocity.

Figure 4 summarizes supply limitation. The wind is not able to pick up sediment in between the vertical dashed-dotted lines, while the wind has capacity to transport more sediment.

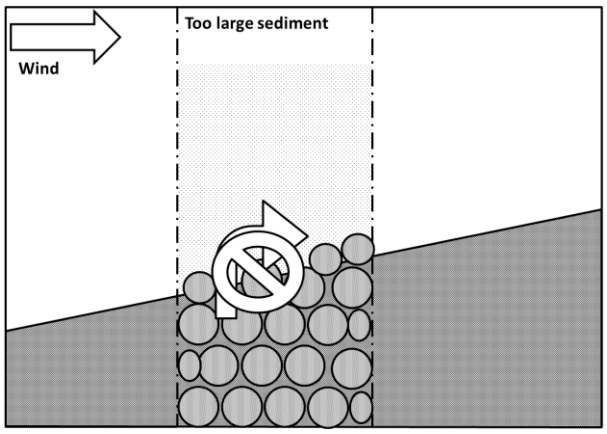

Figure 4; In between the vertical lines the sediment particles are too large to pick up, so the transport is supply limited.

The second limitation is the transport limitation. A certain wind velocity has a maximum transport capacity. When the actual transport is equal to that maximum transport capacity there is saturation. In case of saturation, no more grains can be entrained, because the full capacity of the transport is met. The transport

capacity is dependent on the wind velocity and the threshold velocity. So for pick up, the instantaneous transport has to be smaller than the transport capacity. So, in a situation of transport limitation; there is more sediment availabe than actually is eroded from that bed.

Figure 5 summarizes transport limitation. The wind is not able to pick up sediment in between the vertical dashed-dotted lines, because the wind has reached the maximum capacity to transport sediment.

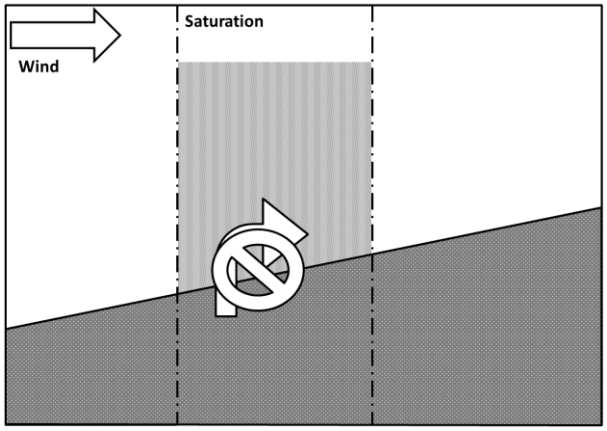

Figure 5; In between the vertical lines the sediment transport is saturated, so the wind cannot pick up sediment from the bed.

A realistic grain size distribution (discretized in the model) is included in the model. For example, a certain wind velocity can pick up a fine grain size fraction but cannot pick up a coarser grain size fraction or a fine grain size fraction can be eroded from the bed and is after a certain time not available anymore but a coarser grain size fraction still is. These examples are a process called sorting of the bed.

The sorting processes can be undone by hydraulic mixing. Hydraulic processes such as wave breaking can mix the top layer of an intertidal beach. The sorting processes affect the grains that are available transport and, therefore, the sediment transport. Furthermore, tide affects the moisture content of the intertidal area and both affect the entrainment of sediment. The wave data is transformed to a local wave height by a maximum wave height over depth ratio (by default is γ=0.50). The mixing depth is a fraction of the local wave height, the empirical depth over disturbance ratio factor (by default is fac_{DOD}=0.10). There is no sediment accreted or eroded, but the sediment is mixed. In the model the mixing of sediment is simulated by averaging the sediment distribution over the depth of disturbance (DOD):

$$DOD = f_{DOD} \cdot \min\left(H_s ; \gamma \cdot d\right) \quad (7)$$

In which H_s represents the local wave height in meters and d the water depth in meters.

The effect of the tide on the sediment transport depends on the drying rate. The sediment in the intertidal zone is sooner available with a small drying rate compared to a large drying rate. When the water level is above the bed level, water will infiltrate in between the grains. When for the same point the bed level is above the water level again (possible for a tide), the water requires some time to disappear. The drying rate is a timescale that represents this disappearing of water by an exponential decay function. The drying time scale indicates the time which is required to dry 50% of the sediment, the halftime. Before the sand is dried, the moisture content increases the threshold velocity and affects the total sediment transport as follows:

$$mc = e^{-\frac{-\log(0.5)}{T_{dry}} \cdot dt} \quad (8)$$

$$mg = \frac{mc \cdot \rho_w}{\rho_p \cdot (1-p)} \quad (9)$$

$$f_{u_{th}} = \max\left(1, 1.8 + 0.6 \cdot \log 10(mg)\right) \quad (10)$$

The moisture content (mc) is determined in (8) and depends on the drying time scale in seconds and decays for every time step dt. The percentage of the dry mass (mg) is determined in (9) with the moisture content, density of water (ρ_w), density of the grains (ρ_p) and the porosity (p). The effect of the percentage of dry mass on the threshold velocity factor (f_{uth}) is determined in (10) and only depends on the percentage of the dry mass. The effect is indicated as a factor. So, the minimal effect (for dry sand) is a factor 1 and the maximum effect of the moisture content is an increase of the threshold velocity with a factor 1.45 (ρ_w=1025 kg/m^3, ρ_p=2650 kg/m^3 and p = 0.4).

3 DATA ANALYSIS

In this chapter the data analysis on Fire Island, New York, USA is described. This analysis was done in cooperation with the United States Geological Survey (USGS). Fire Island data was used in the analysis of aeolian sediment transport. This supplements previous and on-going research at the Sand Motor in the Netherlands. Specifically, this analysis was used to test the AeoLiS. First, the data availability is introduced; after that the analysis is discussed in detail.

3.1 DATA AVAILABILITY

Prior to and in response to the impact of Hurricane Sandy the USGS began a substantial data collection effort to assess the morphological impacts to the beach and dune system at Fire Island. In the following sections data gathered by the USGS and other authorities are further explained.

3.1.1 BEACH PROFILE MEASUREMENTS

Cross-shore and alongshore profiles of elevation data were measured using a geographic positioning system (GPS) surveying instrument. The data were post-processed using positional data from a base receiver. The fixed base station is located on Fire Island. The alongshore profiles are collected at the base of the dune, the mid-beach, and the upper and lower foreshore. The alongshore tracks extend from the eastern boundary of Robert Moses State Park to the western flank of the Wilderness Breach (Figure 6). The 15 cross-shore profiles are spread over Fire Island and extend from just inland of the crest of the dune, if possible, to the low-tide swash zone. This monitoring is on-going and measurements are planned through the summer of 2016. At the time of writing this report, a dataset was available, consisting of 22 different measurements for 10 of the cross-shore profiles; during the period of the 28th of October 2012 to the 21st of January 2016. The other five profiles (profile 28 up to profile 32) have been measured on 13 different occasions; during the period of 12th of December 2013 to 21st of January 2016.

Figure 6; Locations of the profiles on Fire Island (source Google Earth)

Error sources for the GPS data collection can be divided into two categories: uncontrollable random error associated with the signal itself or systematic error associated with the collection of the signal. Since there is no way to control the random error, precautions were taken to minimize the systematic error. To do this the height of the GPS surveying instrument in reference to the land was fixed and measured by hand. There is still the uncertainty for the random error. The vertical uncertainty for the profile measurement is approximately 0.1 meters and the horizontal uncertainty is approximately 1-2.5 meters (Henderson et al., 2015). The uncertainty is treated in more detail in section 5.1.1.

3.1.2 AIRBORNE LIDAR BEACH TOPOGRAPHY OF FIRE ISLAND

Airborne lidar (light detection and ranging) beach topography of Fire Island was collected. The airborne data covers the whole island and not only the dune crest to the swash zone as is the case with the profile measurements conducted by the USGS. Airborne lidar data were gathered post Sandy in November 2012, September 2013, the first week of April 2014 and mid-April 2014. The periods in between lidar measurements were defined as can be seen in Table 2. The lidar data has a vertical accuracy of 15 centimetres. (NOAA, n.d.). A period starts and ends with a lidar data set. The first two lidar data sets consist of gridded data with a resolution of 1.0 meter by 1.0 meter. The third data set has a resolution of 2.0 meter by 2.0 meter and the last data set has a resolution of 0.5 meter by 0.5 meter. The airborne lidar data consist of 'last return' signals. Last return signals are a product of the collection method: during the survey a sensor installed in an airplane sends signals to the land and receives those signals back. Due to reflection by structures or vegetation some signals will return prior to the signals that reach the surrounding surface. Because interest is in the earth surface, 'last return' (also called bare-earth) signals are used and structures and vegetation can be filtered out. The lidar data has a vertical accuracy of 15 centimetres. (NOAA, n.d.).

The lidar data was used to determine changes in volume during the different measurements. Furthermore, cross-shore profiles were extracted from the lidar data to compare with the profile measurements conducted by the USGS.

Table 2; Periods by dividing the lidar data sets

Name	Begin date	End date
Period 1	07-Nov-12	26-Sep-13
Period 2	26-Sep-13	06-Apr-14
Period 3	06-Apr-14	12-Apr-14

3.1.3 WIND AND WAVE BUOY DATA

Wave buoys locations can be seen in Figure 8. Data from wave buoy 44025 was used, rather than buoy 44094 because wave buoy 44094 was only online during the period of 10 February 2014 until 30 July 2015. Although, wave buoy 44094 data helps to validate the modelled wave properties (see 3.2.1). The data of wave buoy 44094 consisted only of wave data and no wind data. Wave buoy 44025 included wave and wind data from 1994 to the present, spanning the post Hurricane Sandy period where USGS measurements were done. At wave buoy 44025 the wind velocity and wind direction were measured every hour by an anemometer five meters above the site elevation. The wave height and the mean wave direction were also measured every hour (National Data Buoy Center, n.d.). The data shows large seasonal variations in wave height. Low waves were observed in the summer with larger waves through the autumn and winter associated with late summer storms and Nor'Easters, storms with winds that generally blow from the northeast. The overall mean wave height is approximately 1.2 meters with a SSE wave direction (Figure 7). The water depth at the location of the buoy is 40.8 meters. The wind data of the MacArthur Airport was discouraged to use by personnel communication with Tim Nelson (USGS).

The wind data from the wave buoy was used to determine an upper limit for the aeolian sediment transport using Bagnold method (3.3) and as input for the AeoLiS model for the Fire Island case in section 4.3. The wave data from the wave buoy is also used as input for the AeoLiS model and to determine Total Water Levels.

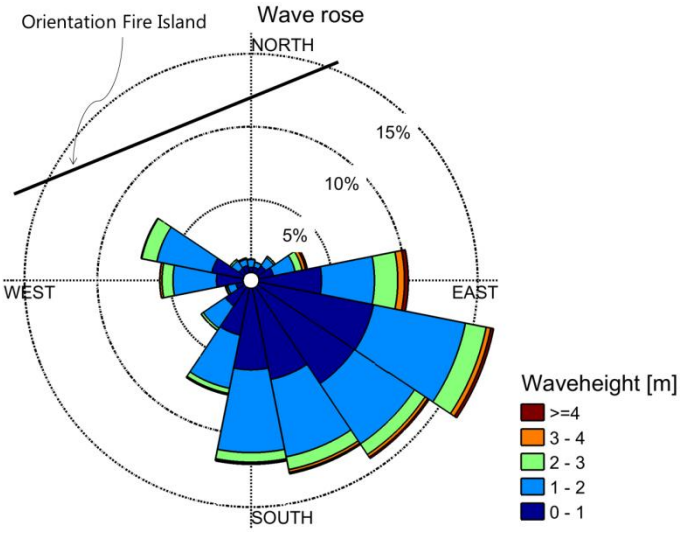

Figure 7; Wave rose for wave buoy 44025

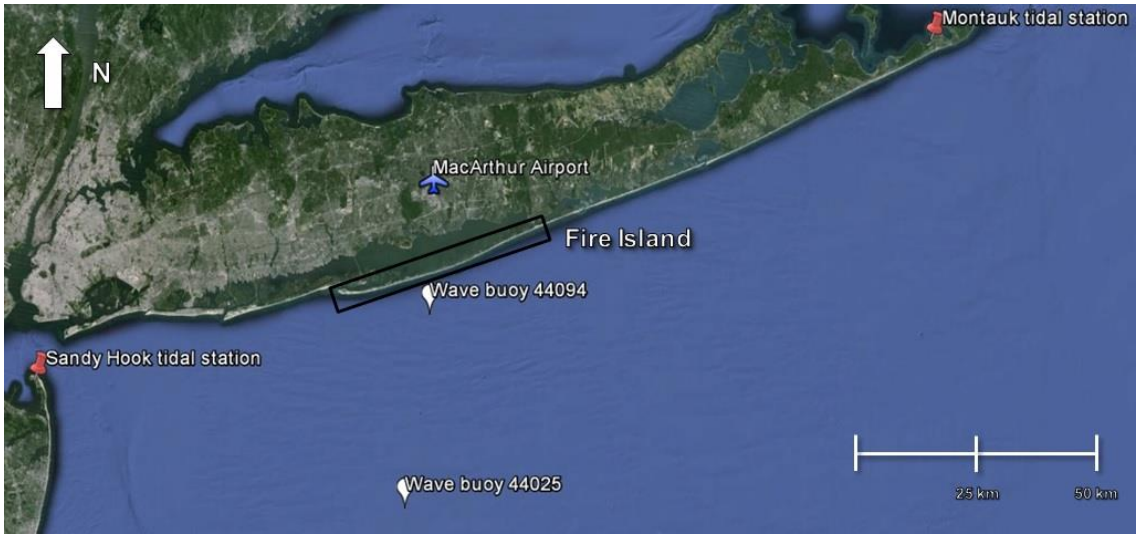

Figure 8; Overview data sources (source: Google Earth)

3.1.4 TIDAL STATIONS

The tidal information for Fire Island is measured at two nearby tidal station. The Sandy Hook tidal station is located west of Fire Island, in New Jersey and the Montauk tidal station is located east of Fire Island, at the eastern end of Long Island, New York (Figure 8). The mean tidal range was observed to be 1.5 meter for Sandy Hook and 0.6 meters for Montauk. The relative large difference is caused by the location in a funnel of Sandy Hook that amplifies the tidal signal. The information from those tidal stations was used to determine the total water level for every cross-shore profile, see 3.2.1. (NOAA, 2013).

3.2 FIRE ISLAND RECOVERY

3.2.1 TOTAL WATER LEVEL

For the transport of sand by wind, the sand has to be dry. So, it was important to determine the total water levels caused by tides and waves. Total Water Level (TWL) combines run up, astronomical tides, and surge. However, these data were not specifically available for the locations of the Fire Island profiles. Therefore, TWL needed to be modelled at each location. The determination of the run-up was based on Stockdon et al. (2006), a parameterization of foreshore beach slope, deep water significant wave height and wave period. Beach slopes were calculated from the cross-shore profile data, collected from 2012 until 2016, and more historical data collected at Fire Island. Acknowledgements have to be made to Kathleen Wilson (USGS) for sharing her knowledge about the TWL.

To accurately inform the Stockdon parameterization, the nearshore wave data at the 20 meter isobath has to be calculated given the offshore wave data (40 meters water depth). To do this, Wilson et al. (in prep.) chose to use an efficient probabilistic time-series construction method (Long et al., 2014). This method makes use of a modelled time-series of wave characteristics (Safak et al., in prep). Nearshore wave characteristics can be determined if there are offshore observations available and a database of deterministic numerical wave model scenario simulations. The available wave data of wave buoy 44094 was used to verify the results from the method.

The tidal data, tidal phase and tidal range, from the two tidal stations were interpolated to the different profile locations on Fire Island. The effect of the location of Sandy Hook station on the tidal amplitude is not considered. However, the linear interpolation is compared to the Tide Table published by Fire Island National Seashore (National Park Service, 2015). Figure 9 shows the predicted MLW tides from Sandy Hook, Montauk, the linear interpolation of the tide and the data points of published high and low tides through the first 9 days of January 2015. The interpolated tide over predicts the published dates, but it appears to be within an acceptable 0.1-m.

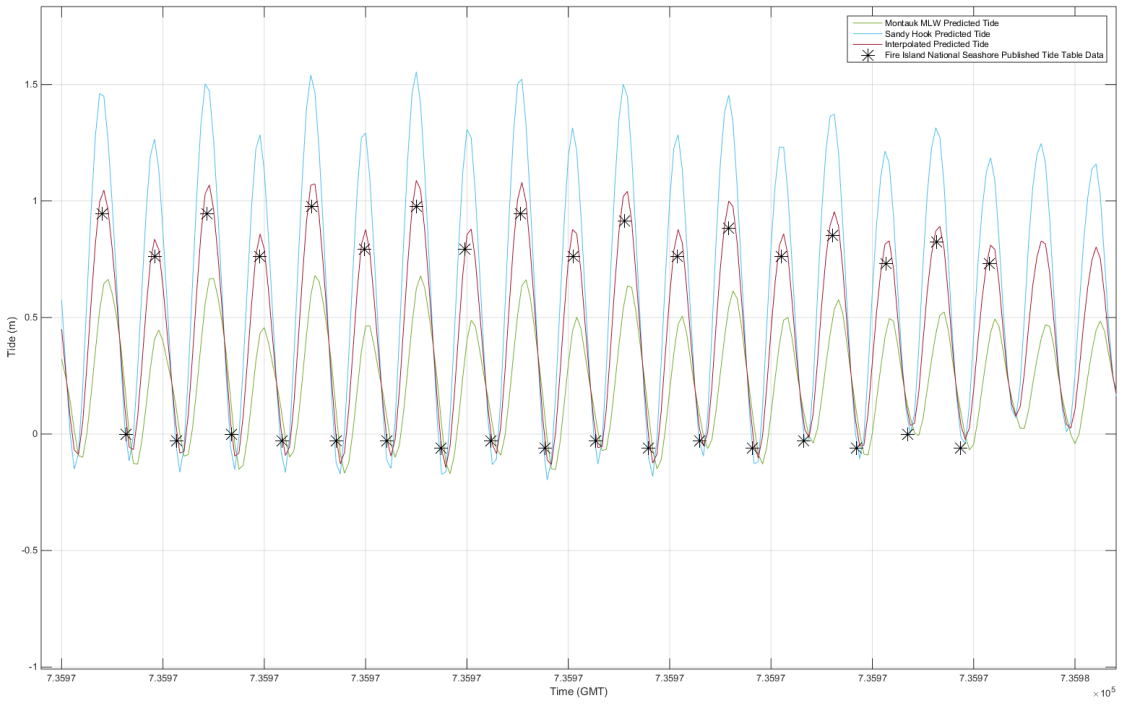

Figure 9; Comparison of the tide at Sandy Hook and Montauk tidal station, the interpolated tide and the data points of the Tidal Table modified from Wilson et al. (in prep.)

In order to account for uncertainty throughout the prediction, including wave and tidal observations, model output and the Stockdon parameterization, a Bayesian Network (a probabilistic graphical model that represents variables and their conditional dependencies) was developed (Plant & Holland, 2011a, 2011b). The Bayesian Network was designed to predict TWL and was trained using the offshore wave conditions, the deterministic model simulations, beach slope and tidal data.

The model generates time series of TWL from which a mean and maximum TWL is determined for every cross-shore profile measured on Fire Island. The TWL time series were generated to correspond with dates of profile measurements. The calculation of the TWL is summarized in Figure 10. Figure 11 shows the results of the determination of the TWL for profile 26, the max TWL with an uncertainty margin and the mean TWL.

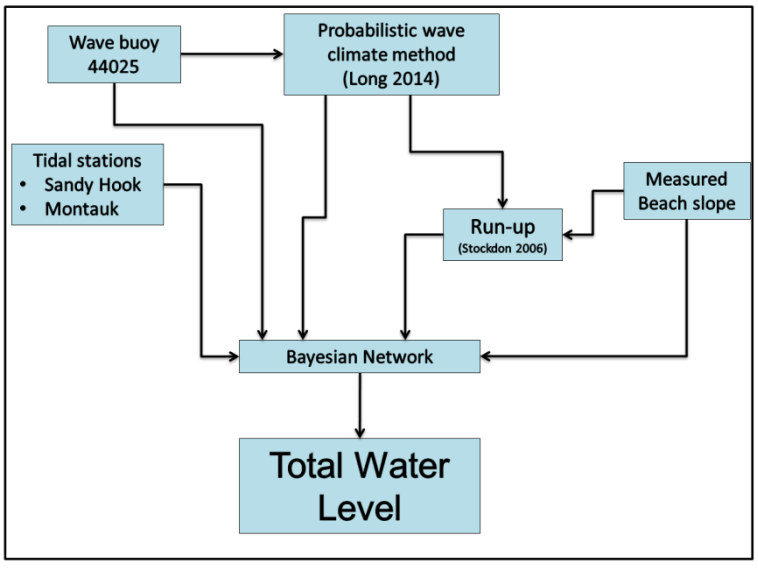

Figure 10; Summary of the determination of the TWL modified from Wilson et al. (in prep.)

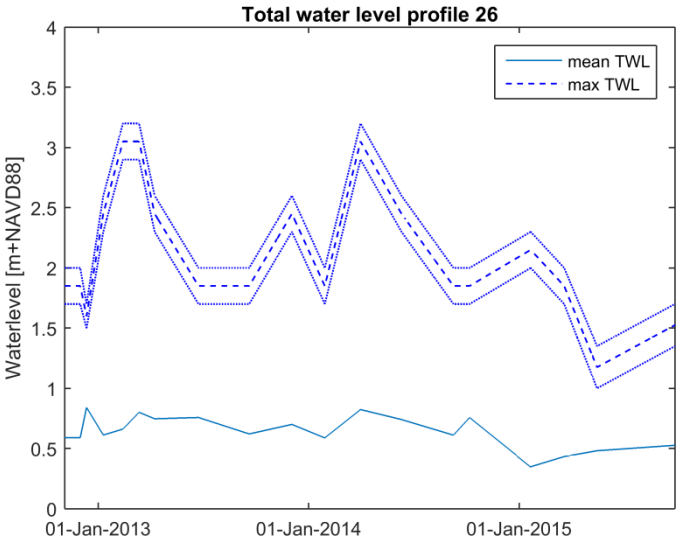

Figure 11; TWL of profile 26 where the dashed indicates the maximum TWL with the maximum and minimum of the corresponding bin from the result of the Bayesian Network; the solid line displays the mean TWL.

3.2.2 CROSS-SHORE PROFILES

The interest areas of Fire Island were chosen corresponding to the profile measurements done by the USGS. Although not all the profile measurements were taken into account. The interesting profiles were located in a natural environment which had very limited intervention of people. So, profiles located in or around communities were excluded. Figure 6 shows the profiles of interest. It has to be noted that profile 22 is located where vehicles can be driven on the beach; this could affect the characteristics of the beach, but it is not clear how or to what extent. At all of the other locations, the beach profile was only influenced by natural behaviour as a result of wind and water.

For all the profiles in Figure 6, the profile measurements conducted by the USGS were used to determine an area of interest. The area of interest is required to make an equal comparison between the lidar data sets. The area of interest had the same dimensions for the different dates of aerial lidar measurements, but the dimensions can change from the one profile to the other. The (eastward) width of an area of interest was approximately 200 meters. Figure 12 shows an example of the interest area of profile 26 for the date of 26 September 2013. Profile 26 is used in all the examples that follow. Other profiles are treated in Appendix A

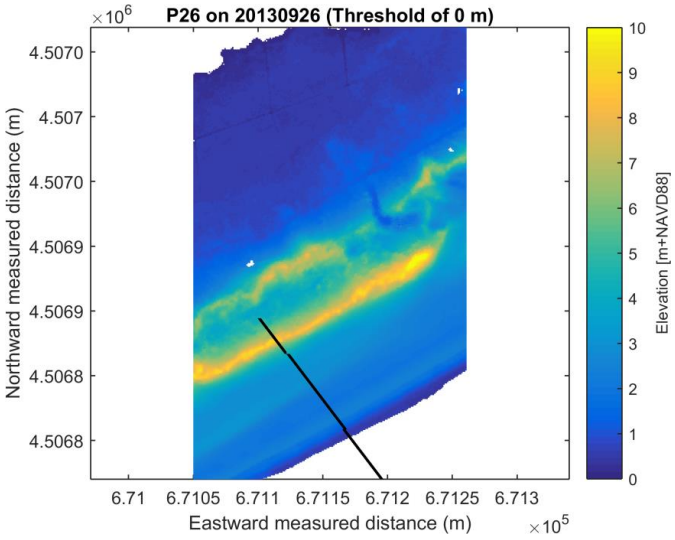

Figure 12; Area of interest of profile 26 09-Sep-13 with elevation above the threshold value of 0.0m. The black line indicates profile 26, where the USGS did its measurements

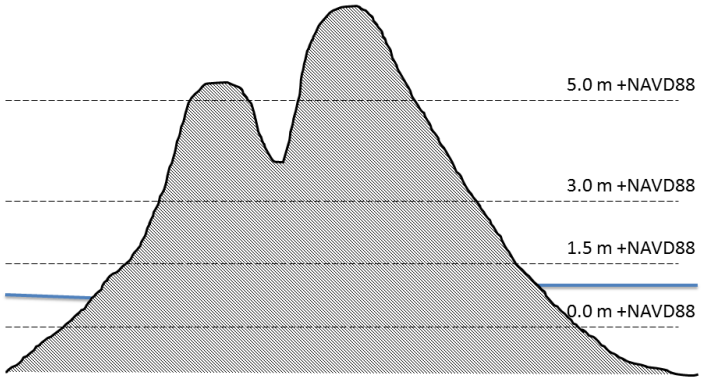

Figure 13; Threshold levels for the areas of interest shown on a generalized schematic of a barrier island cross-section, the water level is indicated by the blue line.

The volume of the island above a threshold elevation value for the area of interest of profile 26 was calculated for the four different airborne lidar measurements. The threshold levels can be found in Figure 13. The smallest threshold of 0.0 meter above the reference level was below the mean high water level of 0.46 m. Topography data below water level contained larger errors in the lidar data and, therefore, those errors are avoided by not taking elevation below 0.0 m+NAVD88 into account. This was also a reason to divide Fire Island in different elevation levels. The threshold level of 3.0 meters was chosen, because this level was the elevation level where the beach was above the maximum TWL and was, therefore, almost always dry. The other thresholds were chosen arbitrarily. The vertical accuracy is 15 centimetres, so, the uncertainty for volumes above 3.0m+NAVD88 has a maximum of 5%. So, the determined volumes have an uncertainty of approximately 5%.

Table 3 indicates the change in volumes with respect to the previous period for profile 26. The changes are displayed in cubic meter per meter. The width of the interest area of profile 26 was 228 meters alongshore. The accretion was an elevation above 3.0m+NAVD88 (3.0m–5.0m+NAVD88 + >5.0m+NAVD88) of 17 m^3/m. The vertical accuracy is 15 centimetres, so, the uncertainty for volumes above 3.0m+NAVD88 is maximal 5%. So, the determined volume of 17 m^3/m has an uncertainty of approximately 5%.

Table 3; Volume change for area of interest of profile 26

Period	Period 1	Period 2	Period 3
Total change [m^3/m]	28	-59	-56
0.0m – 1.5m [m^3/m]	-27	-15	-32
1.5m – 3.0m [m^3/m]	38	-37	-14
3.0m – 5.0m [m^3/m]	13	-6	-6
>5.0m [m^3/m]	4	-1	-3

For Period 2 and Period 3, it can be concluded that there is erosion, because profile volumes decreased for all threshold levels. The erosion for those periods was the same for almost all the areas of interest of the different profiles (Appendix A). So, focus was put on Period 1 because in this period accretion was measured (also in the other areas of interest, see Appendix A). The accretion in the dunes, above a level of 3.0m+NAVD88 is 17 m^3/m.

During the period of accretion, the USGS collected profile measurements for profiles 7, 22, 25 and 26. Due to availability and to begin farthest from communities it was chosen to analyse data from profile 26. However, the other profiles show the same behaviour as for profile 26. That behaviour is discussed below. The results of the other profiles can be found in Appendix A . Figure 14 presents the measured profiles during the period of accretion. The standard deviation for the elevation was determined for the different profiles to quantify the changes in bed elevation. There is a transition zone of relative low standard deviation that separated hydrodynamic dominated and aeolian dominated profile changes. Seawards of that transition zone is a relative dynamic zone most likely due to hydrodynamic processes. Landwards from the transition zone, and above max TWL, is a relative static zone most likely due to aeolian processes and lack of hydrodynamic processes. However, more landwards from the transition zone, the standard deviation increases again and shows also a dynamic zone in the dunes due to aeolian processes. Therefore, the profile can be divided in an area where aeolian sediment transport takes place and an area where hydrodynamic transport takes place as is indicated.

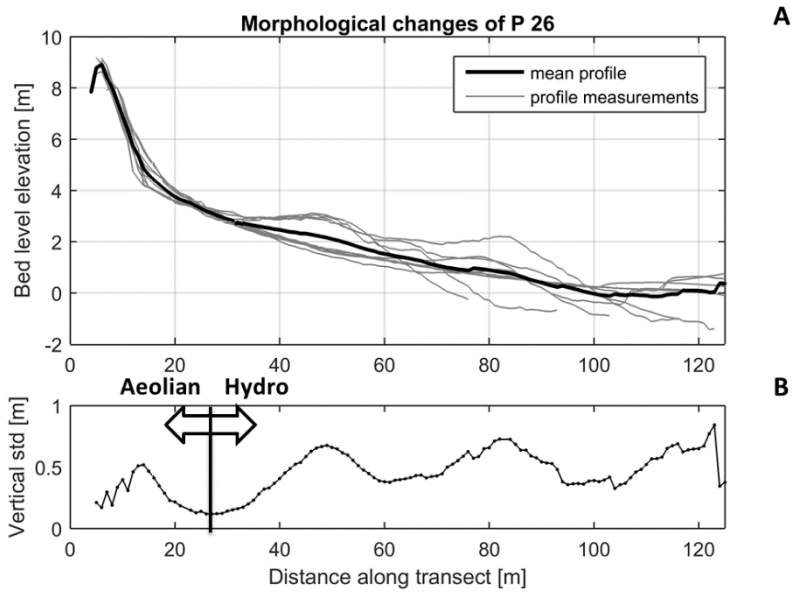

Figure 14; Profile measurements of profile 26; in graph A the black line indicates the mean of all the grey profiles. Graph B shows the standard deviation of the profiles during the period of accretion.

Figure 15A and Figure 16A show the profile change in time and the change of three cross-shore positions in time. The first measurement is white and becomes grey to black during time. Figure 15A shows two cross-shore positions that were arbitrarily chosen in the nearshore zone and Figure 16A shows two cross-shore positions that were arbitrarily chosen in the dune zone. The cross-shore position 1 is the same in both figures

and is between the hydrodynamic zone and the aeolian zone. The profile measurements and the cross-shore elevations in time show that there is a bar welding in the accretion period. The start of the bar welding is indicated by the red dotted line in Figure 15B and Figure 16B. When the bar welding starts, the cross-shore positions CS2 and CS3 in Figure 15B ascend. Figure 15A and Figure 16A show a bar moving landwards in time.

The cross-shore changes are analysed in more detail in Figure 17 and Figure 18. These figures present the change of bed level at the different cross-shore positions with respect to the first and the preceding measurement for the foredune and beach zone. The start of the bar welding is again indicated by the red dotted lines. The graphs which compare measurements with the previous measurement also show the vertical uncertainty of the measurement by the two black horizontal dotted lines. In the beach zone the bed elevation only increased during the welding of the bar and was fairly constant for the rest of the period. The cross-shore elevation changes in Figure 18 show an increase of the dune bed levels after the welding of the bar. So, there is an accretion of the dune after the welding of the bar. The top cross-shore location of Figure 17 is the same as the bottom cross-shore location of Figure 18.

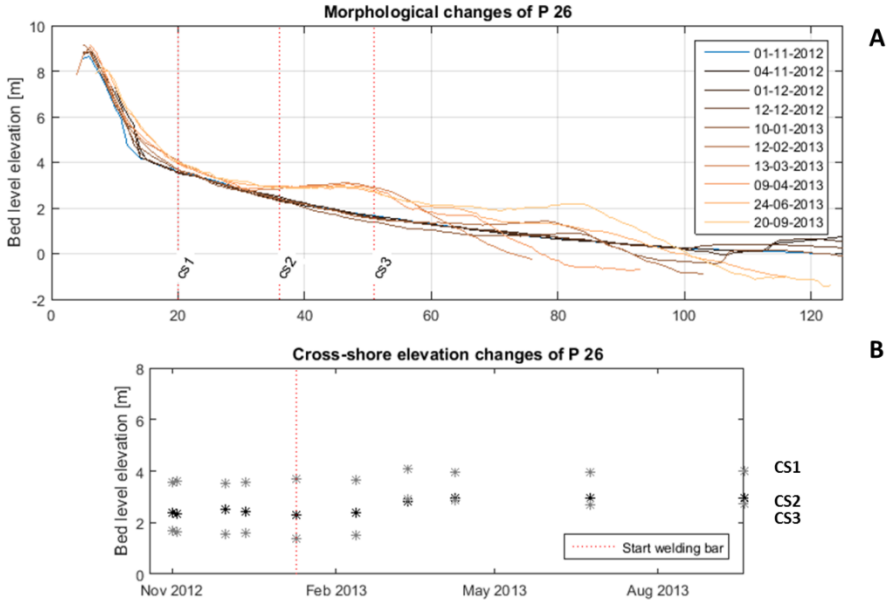

Figure 15; Cross-shore elevation changes in the beach zone for profile 26. The profiles are shown changing in time in graph A. The red dashed cross-shore positions correspond with graph B that shows the cross-shore changes during the accretion period.

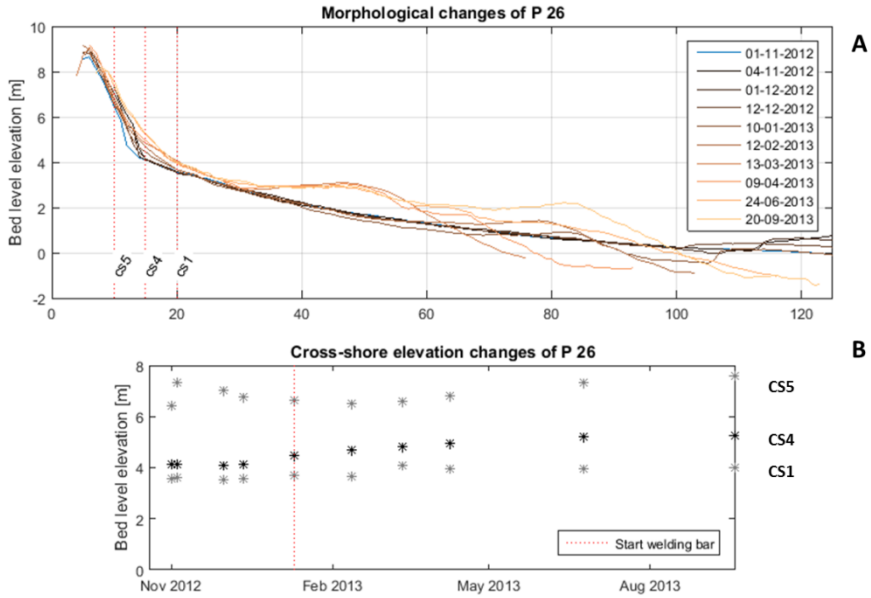

Figure 16; Cross-shore elevation changes in the foredune zone for profile 26. The profiles are shown changing in time in graph A. The red dashed cross-shore positions in graph A correspond with graph B that shows the cross-shore changes during the accretion period.

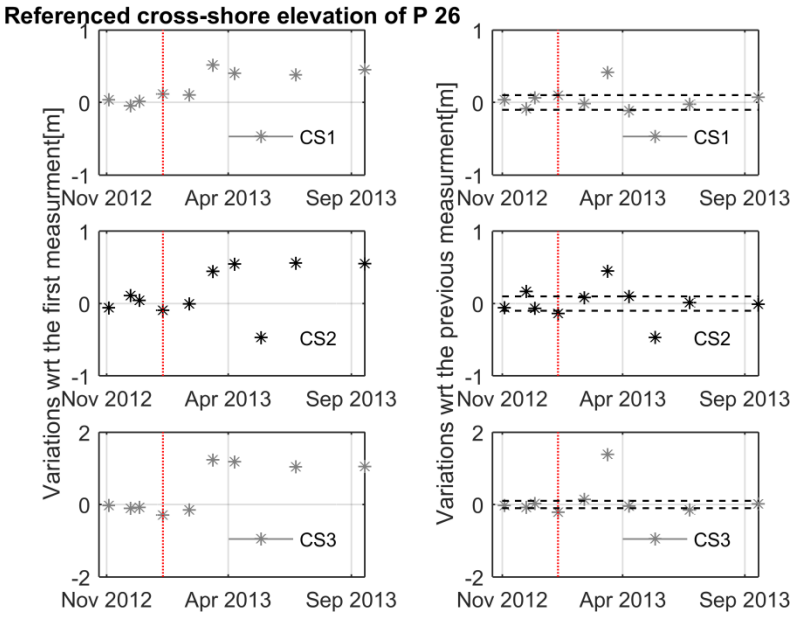

Figure 17;Cross-shore elevations in the beach zone of profile 26. The three graphs on the left show the changes of the bed elevation with respect to the first measurement. The three graphs on the right show the changes of the bed elevation with respect to the preceding measurement, also the vertical measurement uncertainty is included.

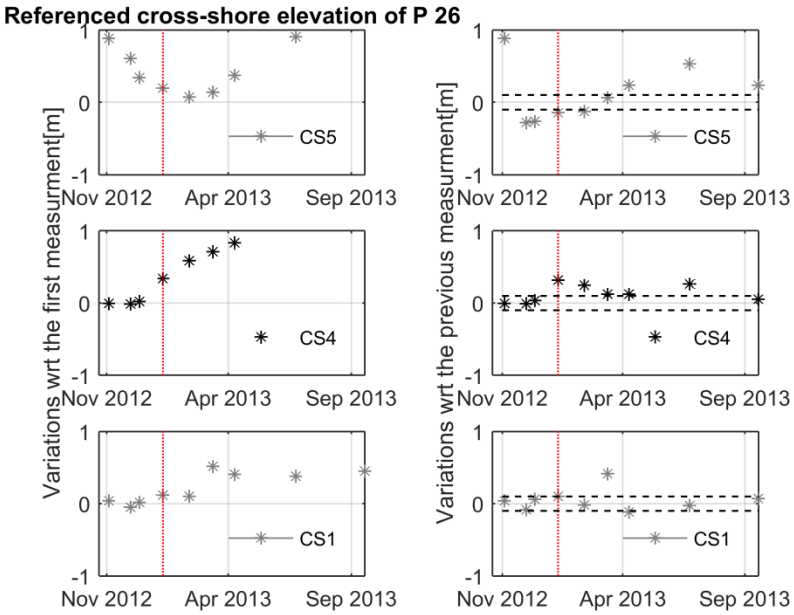

Figure 18; Cross-shore elevations in the foredune zone of profile 26. The three graphs on the left show the changes of the bed elevation with respect to the first measurement. The three graphs on the right show the changes of the bed elevation with respect to the preceding measurement, also the vertical measurement uncertainty is included.

Figure 19 and Figure 20 provide more insight in the horizontal uncertainty of the profile measurements done by the USGS. The profiles measurements itself cannot give that information; so the lidar data at the beginning and at the end of the accretion period were used. The lidar data provided three dimensional data that was required to understand the horizontal uncertainty. 6 Profiles derived from lidar are shown with respect to profile 26 of 1 meter distance. It can be concluded that the hydrodynamic zone (the solid box) was alongshore fairly constant for both lidar data sets. On the other hand, the aeolian zone (the dashed box) was more variable alongshore. The standard deviation for the parallel profiles, indicated Figure 19B and Figure 20B, had the same order of magnitude as the cross-shore changes in bed level measured by the profile measurements in the aeolian zone. So 1-2.5 meter to the right or the left in the lidar data measurement could give the same order of magnitude vertical difference as the successive profile measurements done by the USGS. This is more elaborated in section 5.1.1.

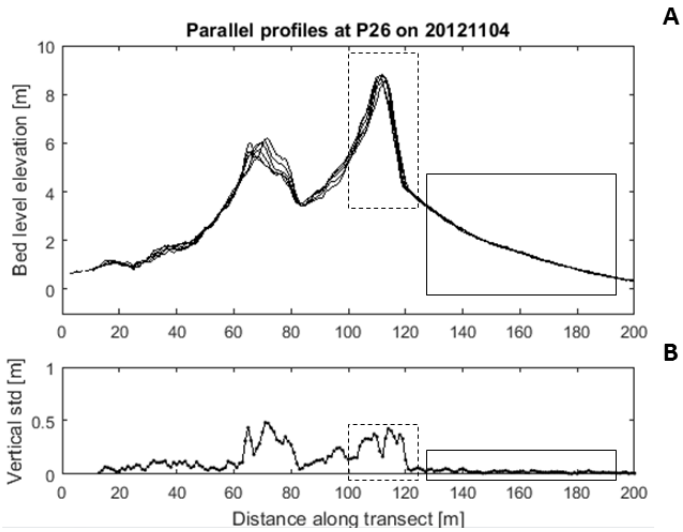

Figure 19; 6 parallel profiles with respect to profile 26 with in between 1 meter distance are shown in graph A for the lidar data set of 04-Nov-2012. Graph B indicates the vertical standard deviation for the elevation for those profiles.

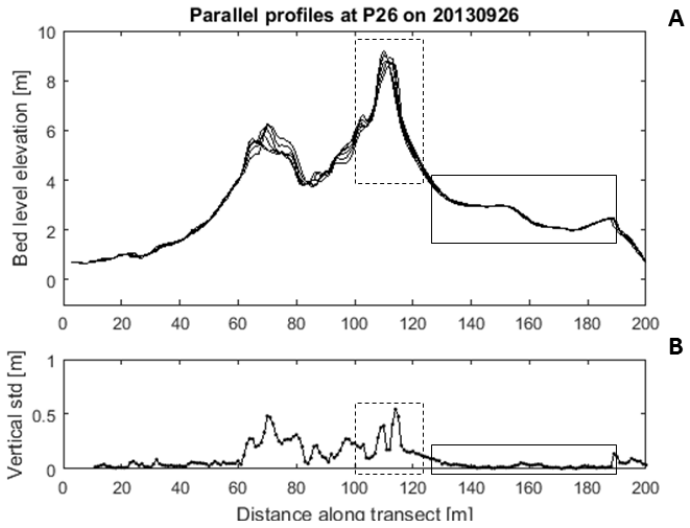

Figure 20; 6 parallel profiles with respect to profile 26 with in between 1 meter are shown in graph A for the lidar data set of 26-Sep-2013. Graph B indicates the vertical standard deviation for the elevation for those profiles.

Figure 21 shows the variation in time of the TWL. It shows an increase in the maximum TWL during the welding of the bar, caused by heavy weather conditions during the same period. The increased TWL is able to migrate the bar landwards. After the welding of the bar the maximum TWL decreased again. The bed levels at the different cross-shore positions are added in this graph. The most seaward cross-shore position (CS3) had an elevation below maximum TWL before the welding of the bar and after the welding of the bar it was above TWL. Therefore, the welding of the bar increased sub-aerial beach.

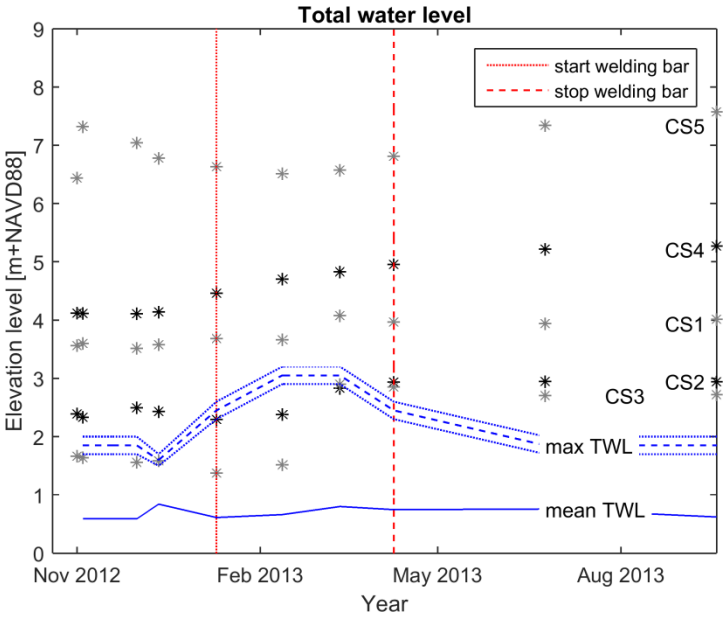

Figure 21; TWL during the accretion period for profile 26. The solid blue line displays the mean TWL, the dashed blue line is the maximum TWL with the uncertainty above and below the maximum TWL. The cross-shore elevations of Figure 17 and Figure 18 are shown as well.

Figure 22 shows in more detail the effect of the welding bar on the beach width. The beach width is defined as the horizontal distance from the waterline to an elevation of 3.0m+NAVD88. The waterline has 4 different values a max TWL, a TWL and a TWL±0.5m representing a time averaged tide. It can be seen that after the welding of the bar the beach width is decreasing because of the temporarily higher water levels. When water levels decreases, the beach width increases to larger levels than before the welding of the bar. It can also be

seen that the beach width for different water levels is less varying than before the welding of the bar. Therefore, it can be concluded that the beach is steeper after the welding of the bar then before.

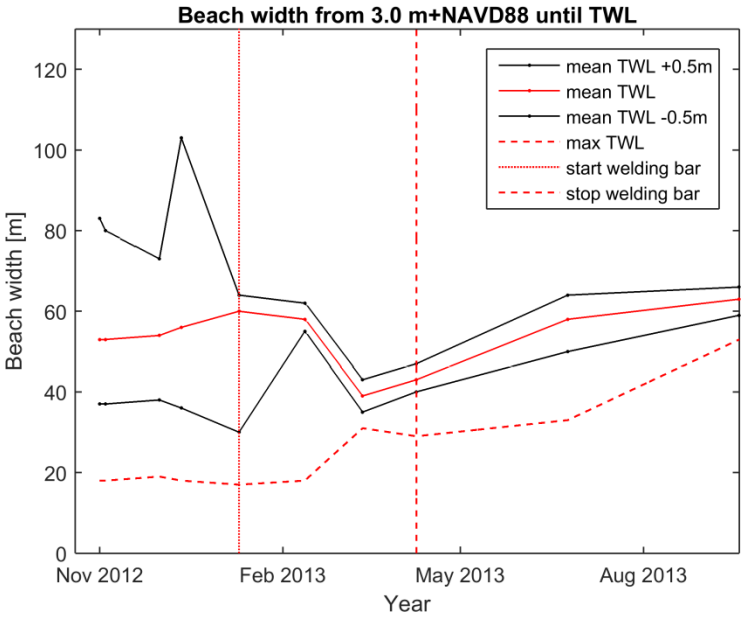

Figure 22; Beach width for the different profile measurements of profile 26. The beach width is measured from the dune toe at a level of 3.0m+NAVD88 until the waterline for four different water levels.

3.2.3 WIND DATA

The wind conditions at Fire Island were assumed to be the same as for the location of the wave buoy 44025 (Figure 8). This assumption can be made, because interest is mainly on the onshore directed wind. For wave buoy 44025 and Fire Island the wind is that case not affected by land. The offshore component of the wind is subject of discussion in section 5.1.2. The wind velocity and direction were evaluated to estimate an aeolian sediment transport potential on Fire Island. The time series of the wind for the accretion period are shown in Figure 23. A relationship between the sediment transport potential and the wind velocity is given by equation (11) introduced by Bagnold. Equation (11) is simplified in equation **Error! Reference source not found.** in a relationship between the sediment transport potential and the wind velocity;

$$q_{eq} = C_b \frac{\rho}{g} \sqrt{\frac{d_n}{D_n}} \left(u_* - u_{*th}\right)^3 \quad (11)$$

A shore normal wind has no correction but every other angle is corrected with the cosine between the shore normal and the wind direction. So, the correction is basically the shore normal component:

$$u_{w,cor} = u_w \cdot \cos\left(\alpha_w - \alpha_{ref}\right) \quad (12)$$

$$q_x = q_{eq} \cdot \cos\left(\alpha_w - \alpha_{ref}\right) \quad (13)$$

The reference angle α_{ref} is 157.5 degrees for Fire Island. The wind direction, α_w, and the wind velocity, u_w, are the measured wind data. This directional correction affected the transport potential, reducing the number of major wind events and reducing the magnitude of these events in many cases. There is a gap of data at the time of January 1st, 2013. Equation (13) indicates how the onshore transport can be determined. So, the onshore component of the total transport is basically determined.

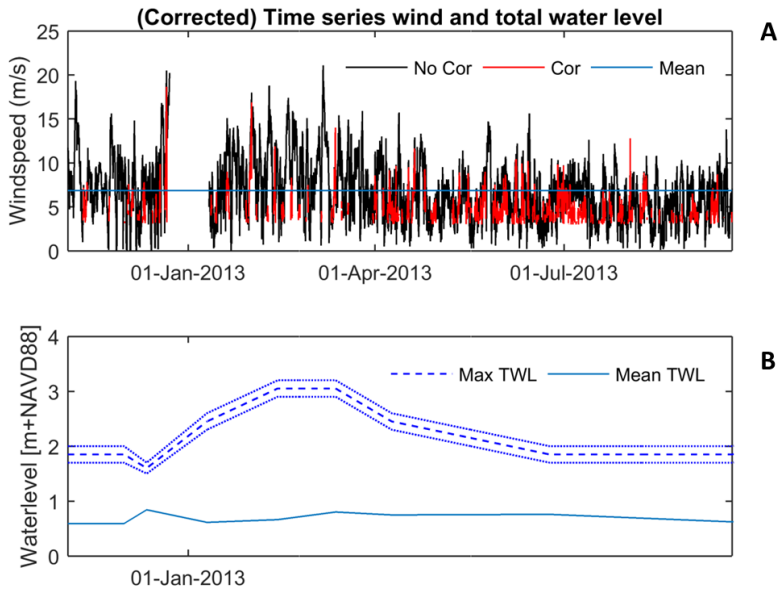

Figure 23; Time series of the wind during the accretion period (07-Nov-12 until 26-Sep-13). The red lines indicate the wind velocity corrected for the wind direction. The mean wind velocity is 6.9m/s and is indicated with the blue line in graph A. Graph B shows the max and mean TWL.

The wind data was also analysed in another way with a wind rose shown in Figure 24. The wind was mostly offshore directed during the total period and the period of interest. Also for the wind rose, the transport potential was determined as shown in Figure 25. This figure as well shows that the contribution of the onshore directed transport potential was minimal compared to the offshore directed transport potential.

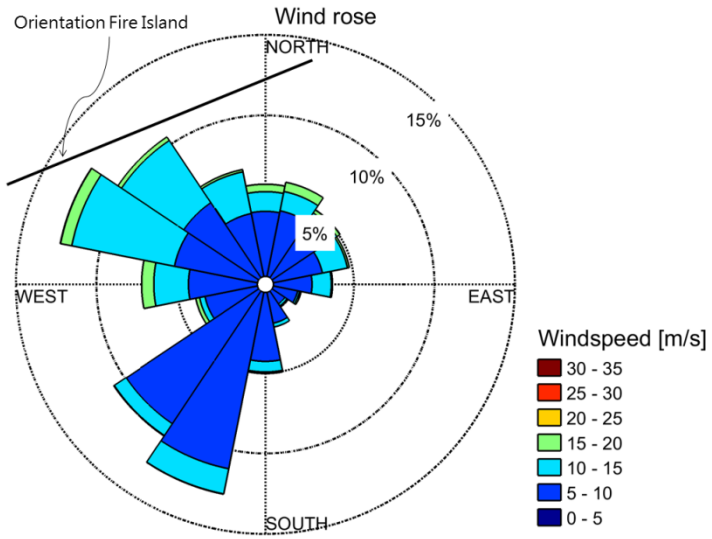

Figure 24; Wind rose of the accretion period (07-Nov-12 until 26-Sep-13) with the orientation of Fire Island included.

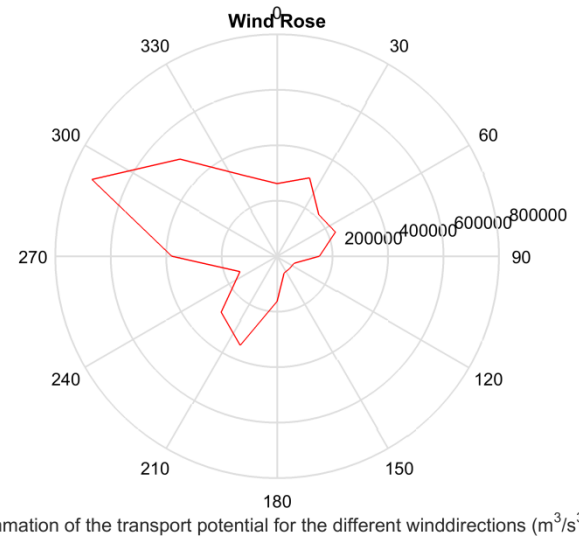

Figure 25; Transport potential for the accretion period (07-Nov-12 until 26-Sep-13).

3.3 TOTAL TRANSPORT BASED ON BAGNOLD

The Bagnold formula is derived for idealized circumstances. It is not including any supply limitation as AeoLiS model is doing. So, the Bagnold formula gives an upper limit for the total transport that can be expected for a certain area. It is interesting to check if the total transport determined by the Bagnold formula makes sense with the dune accretion determined from the lidar data.

The total transport is a summation of all the onshore directed q_x described in equation(13). Input for the equation is measured wind from the wave buoy. The total transport can be determined with equation(14).

$$Total = \int q_x \cdot (1-p)\,\rho_p \cdot dt \quad (14)$$

C_b is the empirical constant depending on the width of the grain size distribution and for normal sorted sediment a value of 1.8 (-) is used. D_n is the reference grain size of 250 µm and d_n the nominal grain size diameter of 500 µm. g is the gravitational constant of 9.81 m/s^2 and ρ_a the density of air. q_x is the summation of all the onshore directed transport for the wind measured at the wave buoy. To be able to determine a volume, the mass is transformed to a volume by using a porosity, p (-), of 0.4 and a density of the grains, ρ_p, of 2650 kg/m^3. The time in between two wind measurements is 600 seconds or 10 minutes; this is the time step, dt.

So using equation (14) as described above the total transport can be estimated. The upper limit for the total onshore directed transport is 31.6 m^3/m. A comparison to the lidar data can be made if the assumption is made that all the onshore transported sediment will settle in the dunes. Then, it can be seen that 31.6 m^3/m is indeed more than the volume of 17 m^3/m determined by the lidar data.

So, it can be concluded that the transport on Fire Island is limited.

3.4 CONCLUSION

The analysis on Fire Island showed that, during the period 7 November 2012 until 26 September 2013 accretion occurred in the areas of interest. The accretion of the dunes was 17 m^3/m (elevation above 3.0m+NAVD88 (3.0m–5.0m+NAVD88 + >5.0m+NAVD88) (Table 3)) with an uncertainty of approximately 5%. In this period the island was recovering from the impact of Hurricane Sandy. During this accretion period a

welding bar was observed. This welding bar could be an important mechanism for the dune growth as accretion was seen in the period after the welding of the bar. The reason for this accretion could be the increasing fetch and the addition of new sediment.

Under idealized circumstances it can be assumed that the total flux settles in the dunes. The determination of the total transport under these circumstances using Bagnold's formulation indicates a larger increase (31.6 m^3/m) than is actually measured. This indicates that the actual accretion of the dunes is limited.

During the study period the wind direction was mainly offshore. It is possible that another mechanism facilitates onshore transport during offshore winds, and may rely on the welding bar as a source of aeolian sediment. Further research is necessary to identify these mechanisms, and local wind measurements at Fire Island would be valuable. Nonetheless, we can use the model to test the possible effect of the increasing fetch and the newly available grains at the shore and the results of model testing can be used to guide future research.

4 SIMULATING AEOLIAN TRANSPORT

In this chapter the simulation results of the AeoLiS model are presented and discussed. The first section introduces additions to the model. The second section introduces and discusses the results of conceptual cases. The third section focuses on the Fire Island case. Data sources described in chapter 3 are used as input for the model. The results of the Fire Island case will be subject to further analysis. The last section compares the results of the model with results of the data analysis.

The focus in this chapter is on beach width and the effect of the fetch on the total sediment transport. Further, sorting and the effect of newly available grains originating from a welding bar are investigated in more detail. This chapter is using the knowledge from the model description provided in chapter 2.3. Appendix B shows an AeoLiS input file where all input is indicated. For the parameters that are not mentioned in this research, the default is used.

4.1 ADDITIONS TO THE AEOLIS MODEL

4.1.1 BAR INTEGRATION

In the model, it is possible to add a bar to the profile such that the effective beach width and grain size distributions are altered by non-aeolian processes. An onshore moving bar can be imposed. Then, on every time step the location of the bar is determined again. It is possible to start or stop the bar at a certain time or place. In between, the displacement can be set. When the bar is imposed, the only variable changing compared to the original profile is the bed level (Figure 26). Figure 26 indicates the onshore bar migration from cross-shore position A to B to C. The solid line is the final bed profile. The dashed lines indicate the profiles before the final profile. The bar migrates 1 meter onshore every hour. The form of the bar is the same during the migration. The blue horizontal line shows the water level. The grain size distribution will not change by changing the bed level. For example, the bar can start migrating landwards after 100 hours model time with every hour a displacement of 1 meter horizontal until 200 hours model time.

Not only is the shift of the bar set, also the form is. The bar is given a standard form; of a Gaussian curve. It is possible to change the height of the bar, the width of the bar (standard deviation) and the location of the centre of the bar. There is one adjustment made to the form. Moving the centre of bar towards the shore there arises a little trough that can hold water, because of the slope of the bed. This trough of water affects the sediment transport. For that reason, the height of the bar from the centre towards the shore is constant. Thus, using this adjusted bar form, changes in beach profiles that are consistent with observed changes can be introduced.

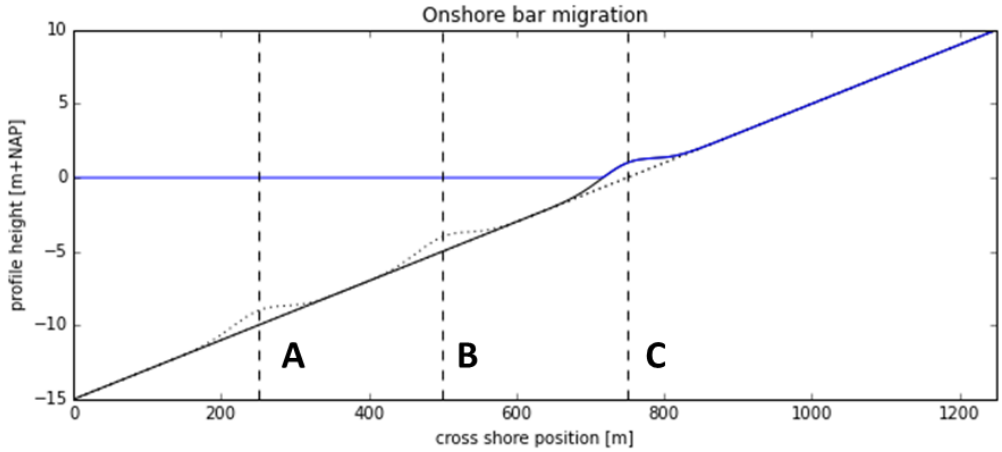

Figure 26; Onshore bar migration from cross-shore position A to B to C.

4.1.2 WIND VELOCITY TIME SERIES GENERATOR

The AeoLiS model is able to do calculations with a constant and a variable wind. This variable wind velocity time series could be created with a generator (Hoonhout, 2015). The generator creates a random wind velocity time series with a prescribed mean and maximum wind velocities, duration and time resolution. The wind velocity time series is generated using a Markov Chain Monte Carlo (MCMC) approach based on a Weibull distribution. MCMC is class of algorithms for sampling from a probability distribution based on constructing a Markov Chain that has the Weibull distribution as its equilibrium distribution. A Markov Chain is a stochastic model indicating a sequence of possible events in which the probability of each event depends only on the state attained in the previous event (Wikipedia, 2016). The shape and scale parameter of the Weibull distribution are set to 2. The wind time series can be written to an input file for the AeoLiS model.

The conceptual cases of section 4.2.5 used a generated variable wind. The mean wind velocity is 6.9 m/s and the maximum wind velocity is 21.1 m/s. This is the same as measured at the wave buoy for Fire Island. The total duration is 1000 hours with a time step of 600 seconds as can be seen in Figure 27.

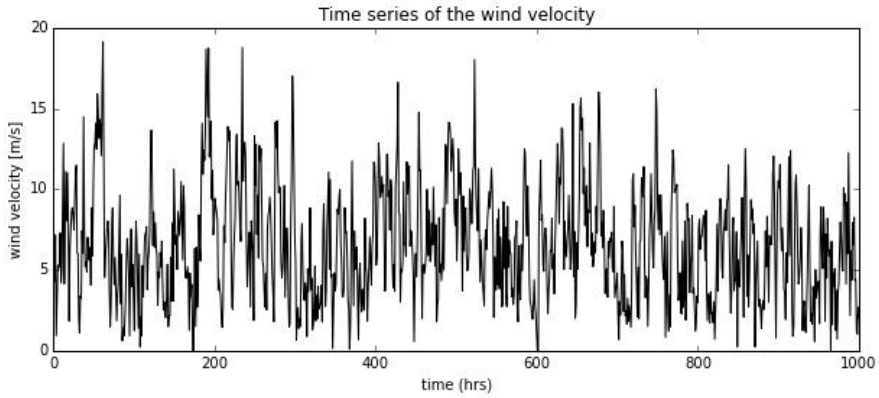

Figure 27; Time series of the wind velocity generated by a MCMC approach based on a Weibull distribution

4.1.3 DETERMINATION MODEL TIME STEP

The time step for a stable model has to be determined. This is done by varying the time step, dt, and compare the results. Figure 28 shows the result of those tests. The relative difference of sediment concentration in the air at the end of the domain at a time of 1000 hours for a certain time step is compared to a time step of 1 second. As can be seen, the difference for a time step of 1800 seconds compared to a time step of 1 second is approximately 0.06%. That is a small value. Therefore, it is chosen to use a time step of 600 seconds to be able to generate enough data.

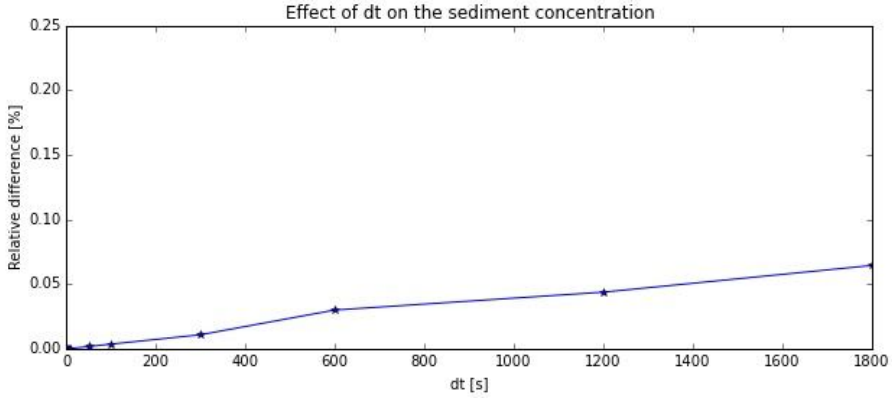

Figure 28; Determination of a time step in the model by comparing relative differences for a varying time step

4.2 CONCEPTUAL CASES

This section discusses 5 conceptual cases to better understand the AeoLiS model and the results of varying some parameters and input (Table 4). Section 4.3 introduces a more complicated case consisting of those parameters and input, therefore they are already introduced separately in this section to minimize complexity. In all conceptual cases, an idealized coast is used (Figure 29 and Figure 40). For all the examples, the initial grain size distribution is a lognormal curve with a geometric mean of 500 µm and a geometric standard deviation of 100 µm (La Selle et al., in prep). The wind direction is in all cases directed onshore.

Table 4; Conceptual Cases

Case	Subject
Conceptual Case #1	Sorting
Conceptual Case #2	Tides and waves
Conceptual Case #3	Adaptation time
Conceptual Case #4	Welding bar
Conceptual Case #5	Variable wind

4.2.1 CONCEPTUAL CASE #1 – SORTING

The first conceptual case models a coast for an arbitrary 1000 hours with a constant wind velocity of 8 m/s, arbitrarily chosen. Figure 29 shows the overview of the conceptual case.

Figure 30 shows the grain size distributions of the bed and in the air at x = 550m, also indicated in the overview, at two different time steps. X = 550m is a location with a comparable horizontal distance from the waterline as the average beach width of Fire Island (Figure 22). It can be observed in Figure 30 that the grain size distribution became coarser during time in the bed at x = 550m and in the air at x = 550m. The relative amount of coarser sediment in the bed and in the air increases over time. This demonstrates the sorting effect; in the

beginning, the wind picks up mainly the relative finer grains. After 1000 hours, there are less fine sediments available, so, the wind picks up coarser sediment.

The total transport and the saturation at x = 550m over the model time of 1000 hours are indicated in Figure 31. The total transport decreases as can be seen in Figure 31. For a particular wind velocity and grain size distribution there is a certain amount of sediment that can be transported. The transport capacity for fine grains is larger than the capacity for coarser grains. So the transport is decreasing, while the transport is saturated for the whole period as can be seen in Figure 31. Sorting causes the decrease in transport. Due to sorting, the relative amount of coarse material increases in the source area.

The total transport as a summation over the modelled time and the time averaged saturation rate of the transport during the modelled time, both in space, are shown in Figure 32. It can be seen that the transport in space is almost constant over the whole beach except for the first approximately 30-40 meters landwards from the waterline. The width of the beach does affect the total sediment transport in this area. If the transport is uniform in space, the transport is fully saturated or there is a lack of supply. In this case, the transport is also saturated. Then it can be concluded that there is transport limitation. The width of the beach does not affect the total sediment transport. So, there is enough supply.

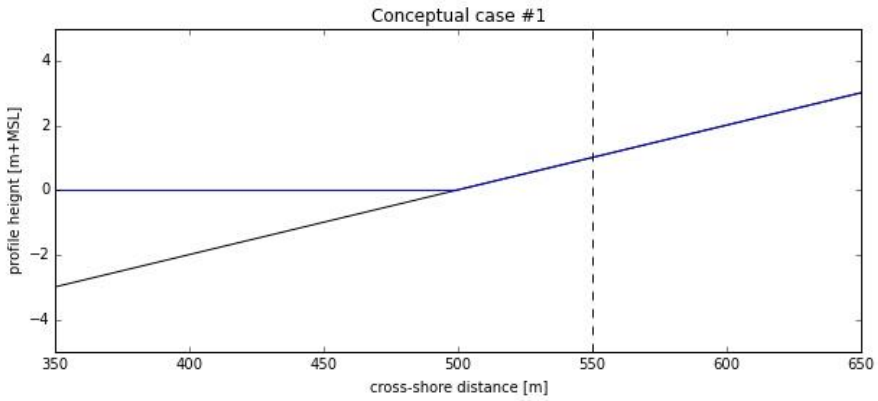

Figure 29; Overview of conceptual case #1, the waterline is indicated in blue. The dashed line is a cross-shore location explained in more detail in Figure 30 and Figure 31.

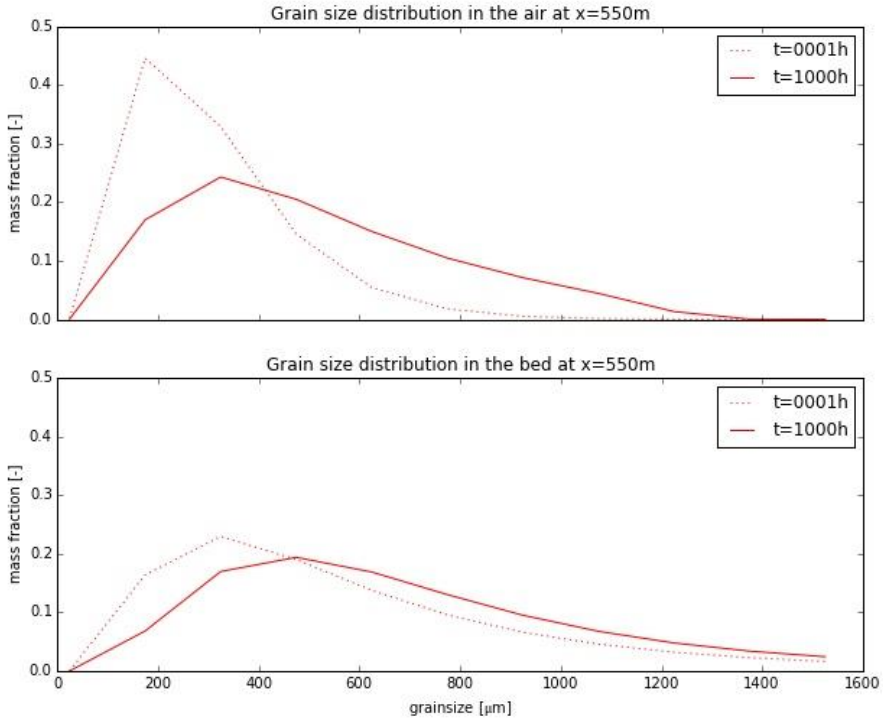

Figure 30; The top graph shows the grain size distribution in the bed at x=550m for t=0001 hours and t=1000 hours. The bottom graph shows the grain size distribution in the air at x=550m for t=0001 hours and t=1000 hours.

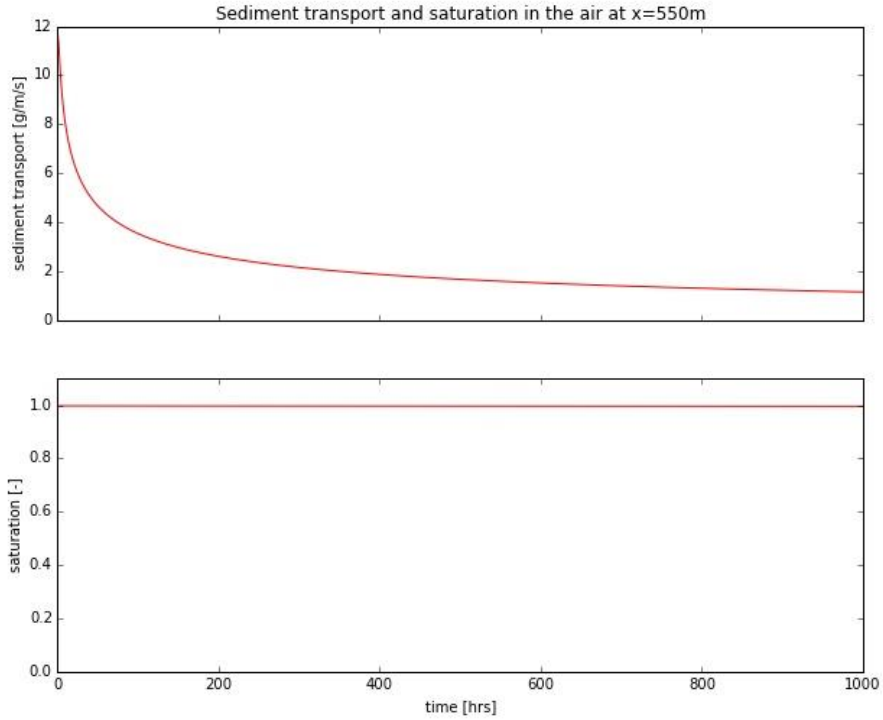

Figure 31; Aeolian sediment transport and saturation in the air at x=550m over time.

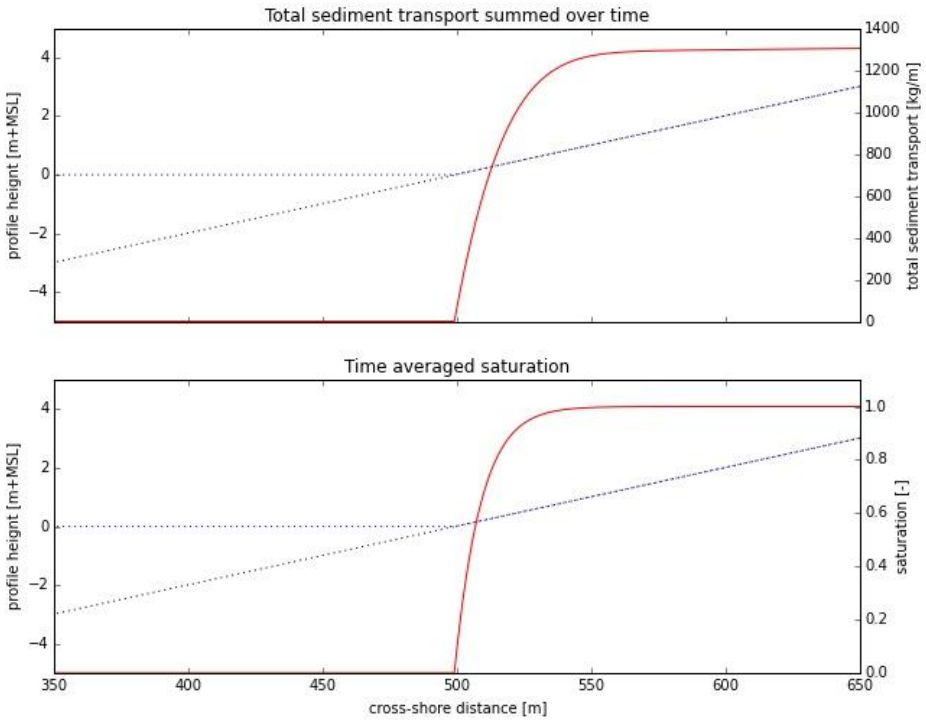

Figure 32; total sediment transport summed over time and the time averaged saturation rate after 1000 hours

4.2.2 CONCEPTUAL CASE #2 – TIDE AND WAVES

Tide and waves affect the model results in different ways. Differences are presented by using a symmetric semi diurnal tide. First the drying rate is tested. When sediment dries quicker, it will be available for transport sooner. This can be seen in Figure 33, Figure 33 shows the bathymetry and the average water level in dashed lines. Furthermore, four lines represent the total sediment transport with different drying time scales. The total sediment transport is summed over time to compare the different time scales. It can be seen that for a smaller time scale the sediment is sooner available for transport and the transport already occurs in the intertidal zone, indicated by the vertical dashed lines. Drying time scales larger than 6 hours will show the same results as for a drying time of 6 hours, because of the symmetric semi diurnal tide and the whole intertidal zone will not dry. It can also be seen that a smaller drying time scales results in larger transport.

A smaller drying time scale results in a larger source area, the intertidal zone, where pick up can occur. So for a smaller drying scale, the wind can pick up more fines from that larger intertidal source area. Therefore, fines cause the larger transport for a smaller drying time scale. The relation between those drying time scales is time dependent. Figure 34 shows the absolute difference between sediment transport for a drying time scale of 1 and 3 hours. The sorting effect increases in time and, then, the sediment availability in the bed becomes more similar. So, the difference in transport for difference drying time scales decreases. To prove the effect of sorting, Figure 35 shows the same different drying time scales for a single grain size. The transport in the intertidal zone is different because of the drying time scale but at the end of the domain the total sediment transport is the same.

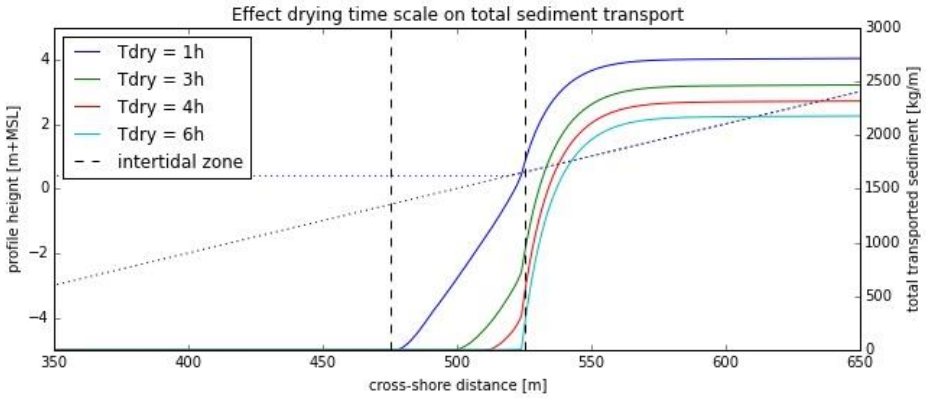

Figure 33; Effect of the drying time scale on transport volumes

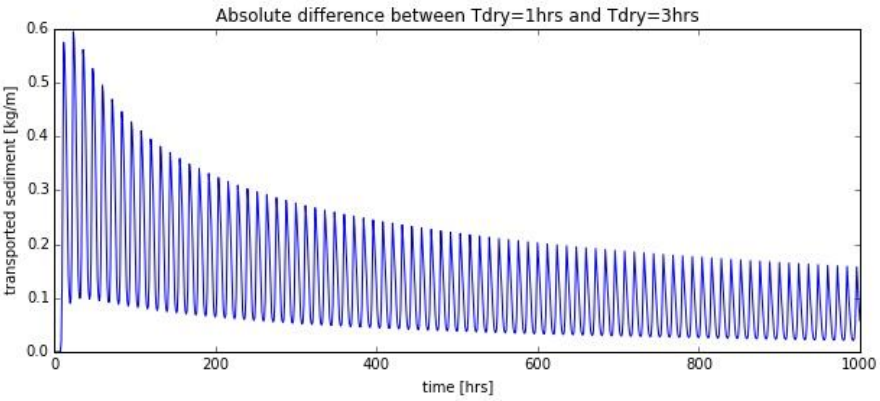

Figure 34; Absolute difference in transported sediment for Tdry=1 hrs and Tdry=3 hrs indicated in time

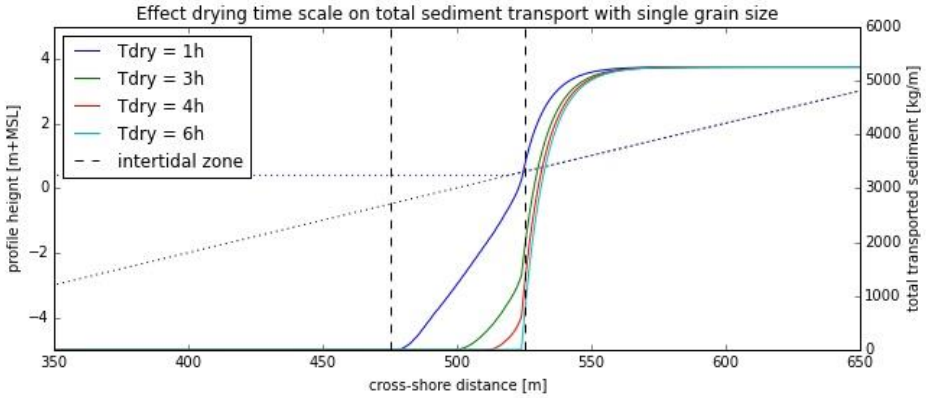

Figure 35; Effect of the drying time scale on transport volumes with a single grain size

The same tests as for the drying time scale are also performed for the tidal range. Figure 36 shows also the bathymetry and the average water level in dashed lines. The different tidal ranges are indicated by the transport curves. The same drying time scale of 3 hours is used. It can be seen that for all three tidal ranges the pick up of sediment starts at the same cross-shore position. The difference in the magnitude is caused by the tidal range. At the end of the domain a larger tidal range causes a larger total transport. This is also caused by the sorting effect. The source area in the intertidal zone is larger for a larger tidal range. So, more fines can be picked up. The difference can be seen in the intertidal zone where the sediment is picked up. To prove the effect of sorting, Figure 37 shows the same different tidal ranges for a single grain size. The transport in the

intertidal zone is different because of the tidal range but at the end of the domain the total sediment transport is the same.

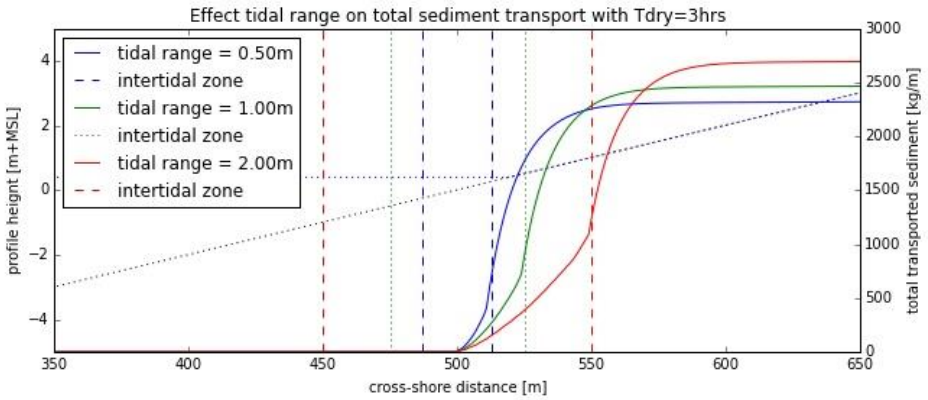

Figure 36; Effect of the tidal range on transport volumes

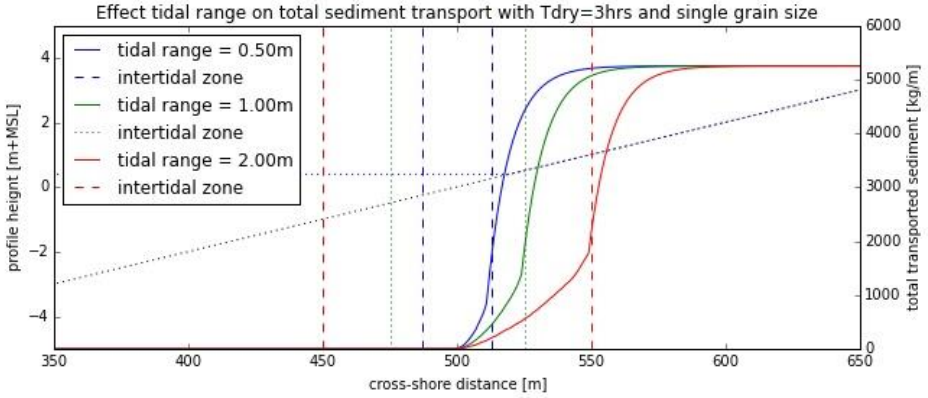

Figure 37; Effect of the tidal range on transport volumes with a single grain size

As mentioned above not only a tide is imposed, but also wave action. Due to wave breaking, the top layer of the bed is mixed. In Figure 38 the effect of wave action is compared to the case without wave action. A tidal range of 1.00m is imposed with a drying time of 3 hours. The bathymetry and the average water level are indicated in dashed lines. The transport curves for both cases start at the same cross-shore position but do not have the same magnitude. Due to mixing, the total transport will increase. The effect of waves will be larger for a larger tidal range and a smaller drying time scale, because the intertidal source area increases. The difference in transport is caused by sorting. Showing a figure with a single grain size will give the same transport for waves and no waves, because the sediment of the same size is mixed.

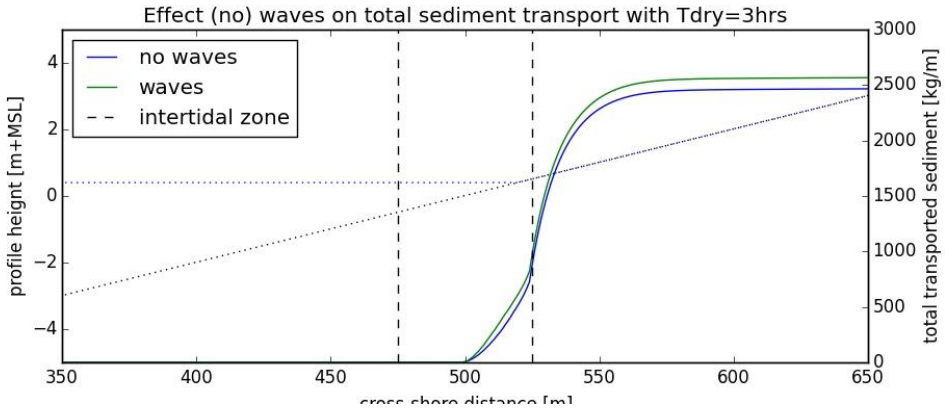

Figure 38; The total transported sediment for the cases with and without wave action compared

4.2.3 CONCEPTUAL CASE #3 – ADAPTATION TIME

In Chapter 2.3 adaptation time is introduced. The adaptation time scale represents the time the instantaneous sediment concentration needs to adapt to the equilibrium sediment concentration. Variations of the adaptation time are indicated in Figure 39. The bathymetry and the average water level are indicated in dashed lines. The different transport concentration curves after the first time step (1 hour) are shown in different colours. For an increasing adaptation time scale more space is required to adapt to an equilibrium sediment concentration. Fire Island beach has an average width of approximately 50 meters. It can be seen for the dashed vertical line that not for all the adaptation time scales equilibrium is reached. Although, the expected value for the adaptation time scale is in the range of 0.5 seconds – 2.0 seconds. So, the displayed adaptation time scale of 5.0 seconds is not realistic and only shown to explain the effect of variations in adaptation time scales.

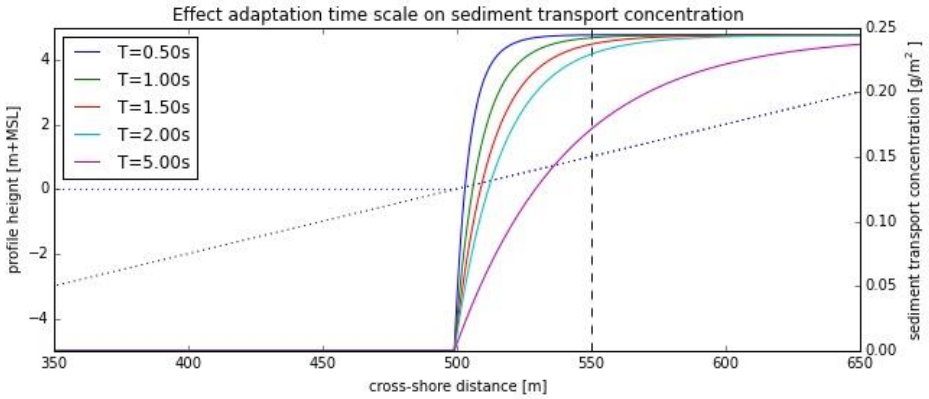

Figure 39; Effect of variations in the adaptation time scale on the sediment transport concentration at t=001h

4.2.4 CONCEPTUAL CASE #4 – WELDING BAR

The fourth conceptual case also models a coast for 1000 hours. The wind is constant with a velocity of 8 m/s, arbitrarily chosen. The difference with Conceptual Case #1 is the welding of a bar as can be seen in Figure 40 (section 4.1.1). The grain size distribution is shown in the same way as for conceptual case #1 (Figure 31).

Figure 41 shows the effect of the welding bar on the grain size distribution of the sediment in the bed at two different locations in more detail. The first location is located at x=475m and is the location of the welding bar. So, before the welding of the bar this location is below water level and after the welding of the bar this location is above water level. The second location is x=550m and is the original beach. The grain size distribution in the bed is shown at the moment the cross-shore location is above water. The grains in the welding bar have the same grain size distribution as the grains on the beach at the first time step. But at the moment grains were below water level they could not be picked-up by the wind. After the welding of the bar, the pick up of that sediment is possible. The welding bar makes new finer grains available for transport.

Conceptual case #1 discusses the effect of sorting on the total sediment transport rate. Figure 42 shows that the welding bar affects the total sediment transport as well. An increase of the sediment transport can be observed in case of welding bar which makes new grains available. The sediment transport is still saturated for the whole period.

Another effect on the sediment transport rate can be caused by the increase of the fetch. The welding bar increases the fetch. Figure 42 shows also the saturation of the conceptual case prior and post welding of the bar. In both situations the sediment transport rate is saturated. So, the transport is transport limited.

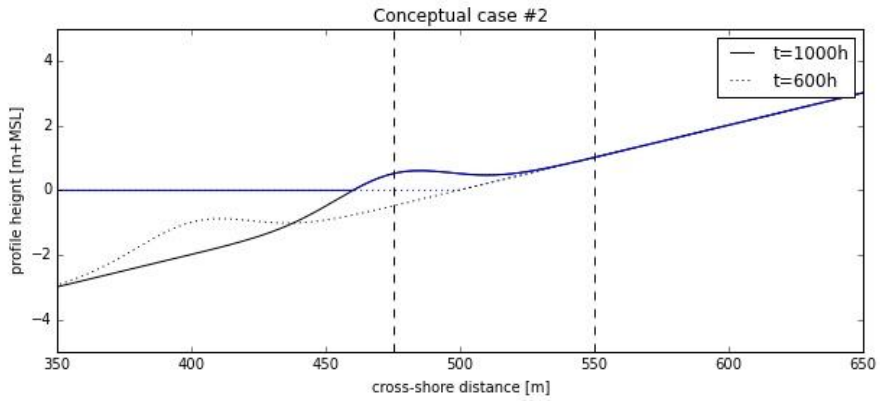

Figure 40; Overview of conceptual case #4 and #5, the waterline is indicated in blue. The welding bar is indicated at t=1000 hours and the dashed welding bar is indicated at t=600 hours. The dashed vertical lines are cross-shore locations explained in more detail the figures below.

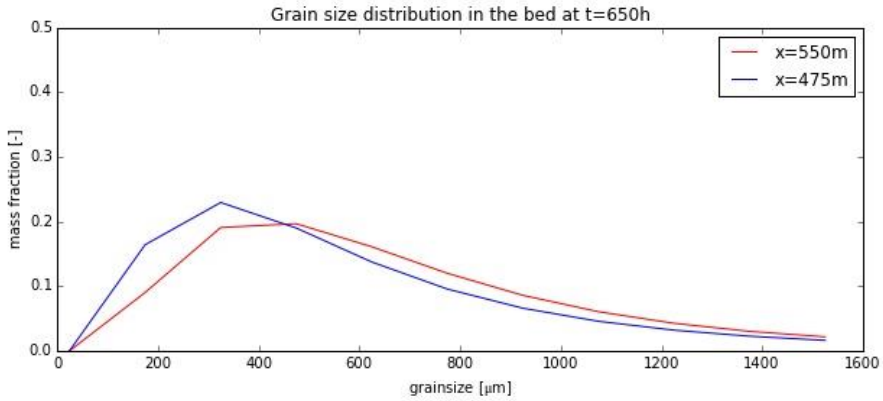

Figure 41; The grain size distribution is indicated in the bed at x=475m and x=550m for t=650 hours after the welding of the bar.

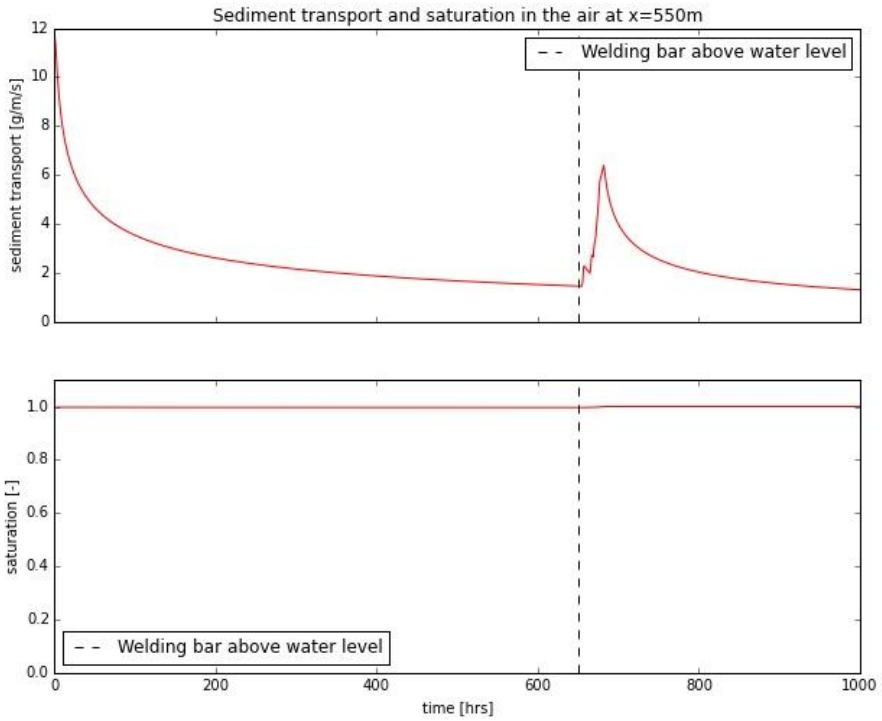

Figure 42; The sediment transport rate at a particular time in the top graph in case with and without the welding the bar at the location x=550m. The bottom graph indicates the time averaged saturation in the air at x=550m.

4.2.5 CONCEPTUAL CASE #5 – VARIABLE WIND

The fifth conceptual case is also modelled for 1000 hours. As for conceptual case #4 also in conceptual case #5 a welding bar is imposed (Figure 40). The difference with the previous conceptual case is that a variable wind with a mean velocity of 6.9 m/s is used, generated by the wind generator (section 4.1.2, Figure 27). The mean velocity in this case is the same as the mean velocity measured for the Fire Island case. The welding of the bar causes the same effect on the grain size distribution as for conceptual case #4 (Figure 43). Again there are two cross-shore positions chosen which show their grain size distribution at the moment the cross-shore position of x=475m gets above water. That cross-shore position is compared to x=550m.

Figure 44 shows the relative increase of transport by comparing a case of variable wind with and without a welding bar. The results are indicated with a rolling mean and an actual difference. Also in case of a variable wind, the welding of the bar causes an increase of the sediment transport. However, the increase of transport is small. The cause of the increase is more variable than the previous conceptual case. When the wind velocity is changing also its transport capacity is changing. The rolling mean is added in Figure 44 to show the relative trend, because due to the changing wind velocity the actual difference contains a lot of wiggles.

The effect of the fetch is shown in more detail in Figure 45. The bathymetry and the water level are shown at the last time step in both figures. The transport is not saturated but it reaches a level of almost 1.0. This level is an average over time. So, it indicates that for most of the time the transport is saturated and transport limited. However, the saturation can also be smaller than 1 and, then, the transport is supply limited. If the wind velocity is small it is possible there are not enough fines available to pick up. Then the saturation is less than 1. The shape of the transport and saturation curves is caused by the welding bar that is not available the whole period, but only after approximately 650 hours.

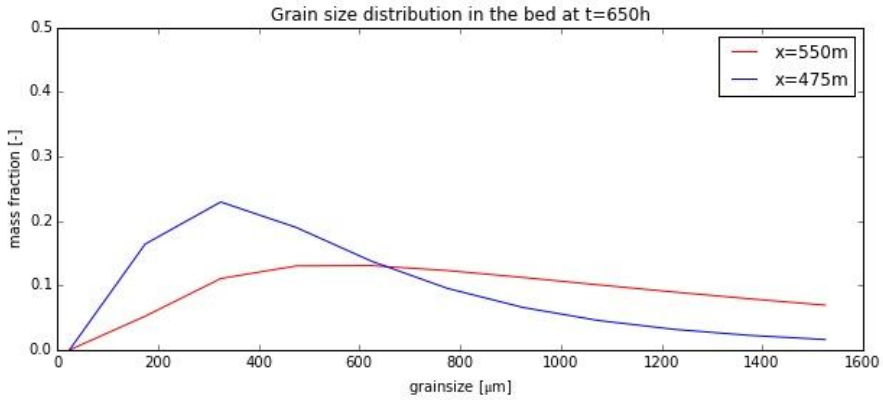

Figure 43; The grain size distribution in the bed at x=700m and x=800m for t=700 hours after the welding of the bar.

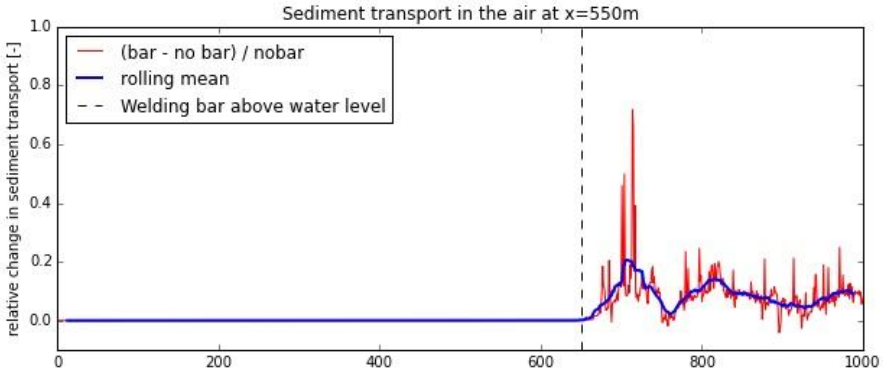

Figure 44; The relative increase of aeolian sediment transport in the top graph is determined by comparing the sediment transport with and without the welding the bar with respect to the case without the welding bar at the location x=800m. The rolling mean is an average value over time and is indicated in blue. The increase of transport occurs after the welding of the bar.

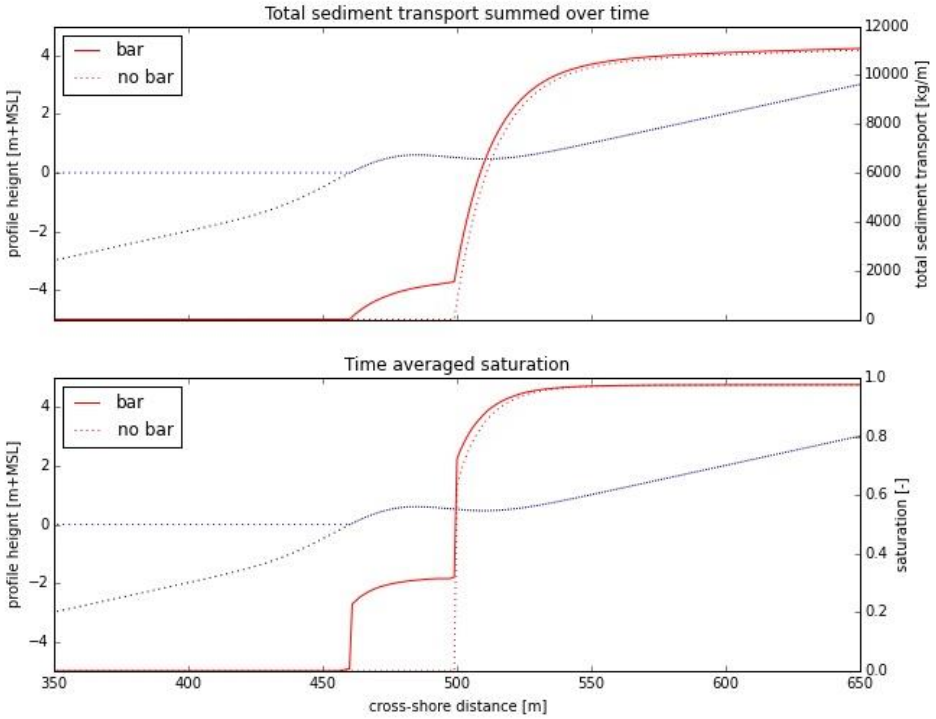

Figure 45; Total sediment transport and the saturation of the sediment transport for the case with and without a welding bar.

4.3 FIRE ISLAND CASE

In this section, modelling is continued on the Fire Island case. Data of Fire Island (Chapter 3) is used as input in the model. The profile measurements conducted by the USGS are imposed on the model. Therefore, the bathymetry changes 8 times during the model time. The model time is equal to the accretion period, Period 1, as described in Chapter 3. The wind (corrected for direction such that only the onshore component is used by the model and the wind was measured at a height of 5 meters) and wave data, originating from wave buoy 44025, are input as well. In this chapter, only the onshore flux is taken into account, because we are interested in onshore transport.

Furthermore, a changing mean of the TWL is used in combination with a symmetric semi diurnal tide. The tidal range is 1.0m (section 3.1.4). To determine the transported volume, a density of 2650 kg/m^3 is used for the sediment with a porosity of 0.4.

There are no measurements done to determine the grain size distribution at Fire Island. So, an educated guess is used. The grain size distribution is the same as for the conceptual cases, a lognormal curve with a geometric mean of 500 µm and a geometric standard deviation of 100 µm (La Selle et al., in prep). Results from the model are gathered at the point where the elevation is approximately 3.0m+NAVD88 (Figure 47). In the next section, the grain size distribution and also the fetch and the adaptation time are subject to further analysis.

The first results of the Fire Island case are shown in Figure 46. Every period in between two measurements conducted by the USGS the bathymetry and the mean TWL for that period are shown. So, the first period starts with a bathymetry shown in the top left plot and the last period starts with the bathymetry of the bottom right plot. Every period has a different length in time. The total transport for every period is indicated in red. It can be seen that the magnitude of the total transport is varying; the first period shows even no

transport at all. Besides, the transport curves are not uniform at the end of the domain, which indicates that the transport is not saturated and that the length of the fetch affects the total transport (supply limitation). To be able to better compare the different periods, the day averaged total transport are shown. The third and fourth period (30-70 days and 70-104 days) show the largest magnitudes. This is also the period just before and the start of the welding bar as was indicated in Chapter 3. That period was also the period with the strongest wind (Figure 23). Figure 22 showed that the beach width increased during the bar welding and the period after that. Figure 46 shows only the larger transport during the welding of the bar and not in the period after that. So, it more likely the increase transport is caused by the stronger winds.

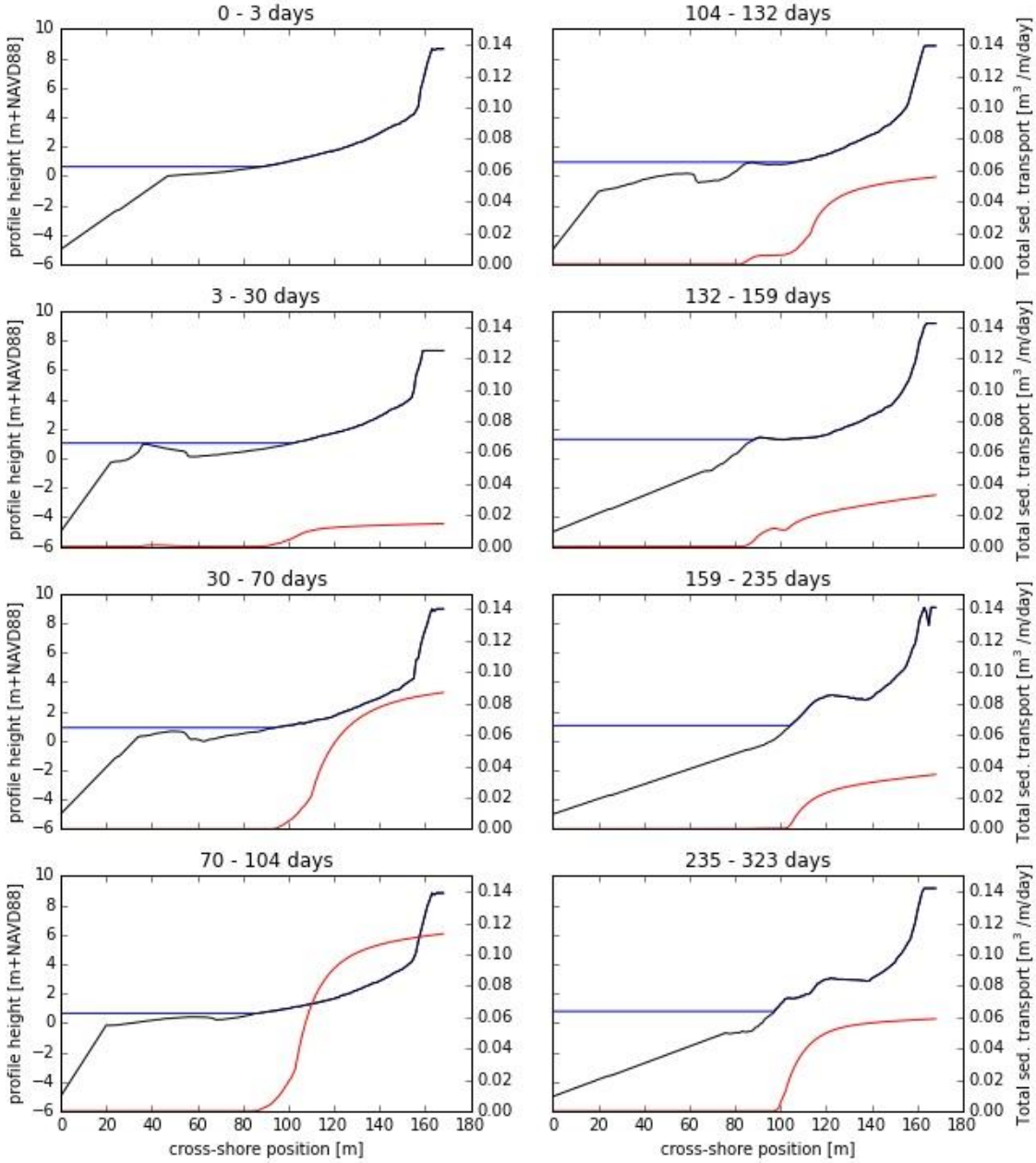

Figure 46; Total day averaged transport in between measurements conducted by the USGS

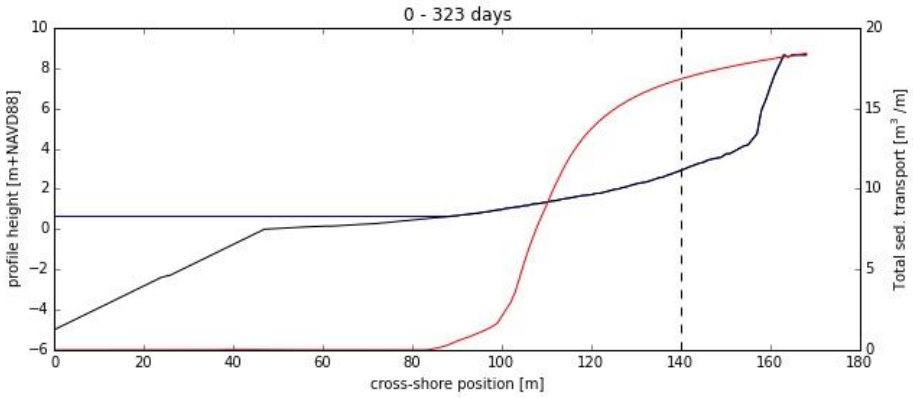

Figure 47; Total transport summed over the periods

Figure 47 shows the summation over the 8 periods and, so, the total transport for the whole accretion period. The bathymetry and the mean TWL of the first measurement are indicated as well. The dashed vertical line indicates the cross-shore position where the bed elevation is 3m+NAVD88. It can be seen that the total transport curve is increasing in space and is not uniform as for the conceptual cases.

For that reason it is interesting to have a look into the saturation rate of the onshore sediment transport. Figure 48 shows again the bathymetry and the mean TWL for every period in between measurements conducted by the USGS. For every cross-shore position, the median saturation rate is shown. The median is chosen because the average is too much influenced by peaks in the saturation. These peaks are caused by changes in wind velocities. Therefore, saturation rates can reach very large values or even infinity. In the first period there was no onshore sediment transport, so, there is also no saturation. In all other periods, it can be seen that the saturation rate increases from zero to approximately 1. Some periods show some wiggles in the intertidal zone. The wiggles do not affect saturation rate landwards transport.

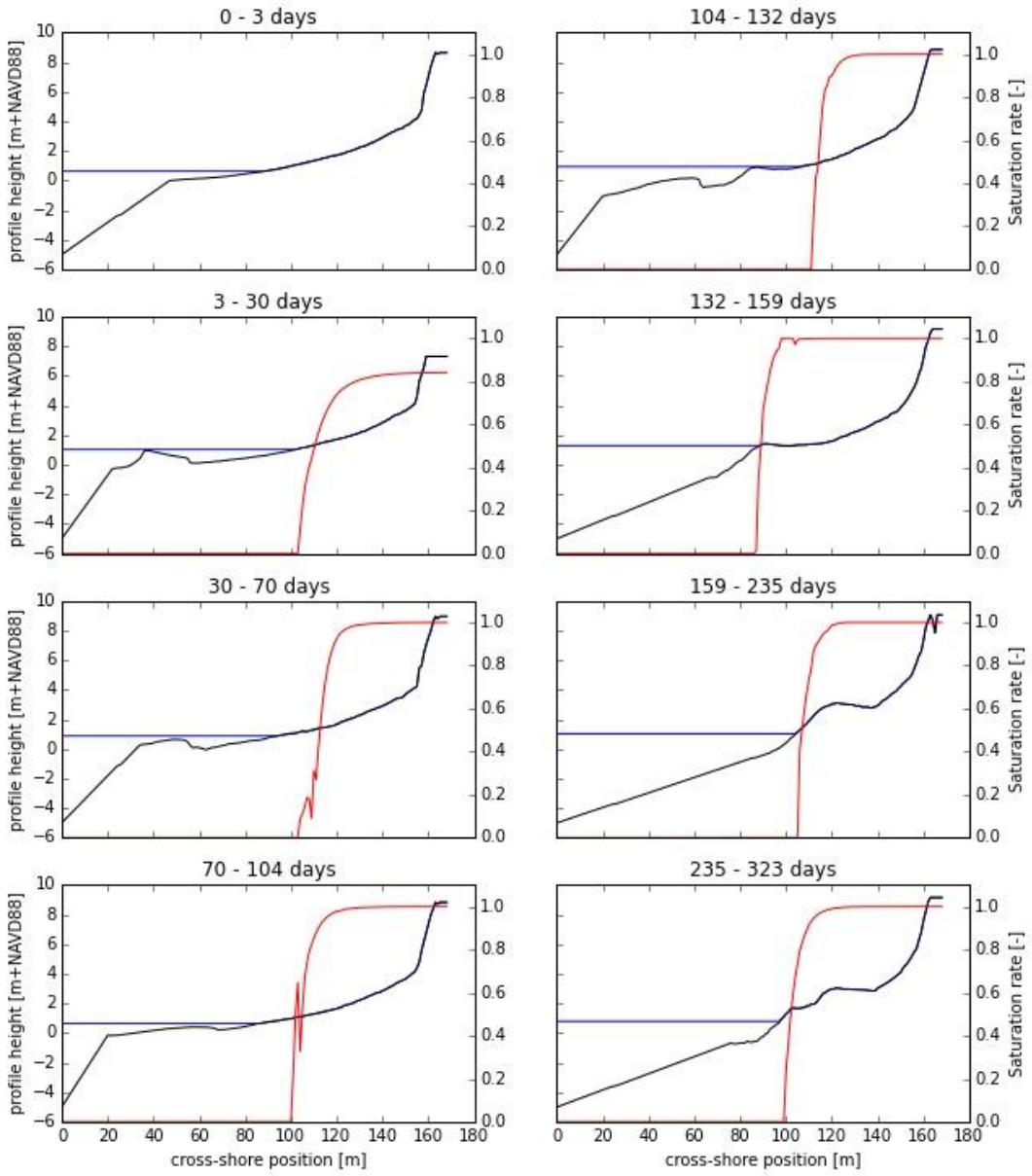

Figure 48; Saturation rate in between measurements conducted by the USGS

Figure 49 shows the median of the saturation rate over the whole period. The bathymetry and mean TWL of the first measurement are also shown. It can be seen that the saturation over the whole period show the same results as for the separate periods. At x=140m it seems that in all the plots the saturation rate is approximately 1.0. That would be interesting, because for a saturation of 1.0 a uniform total transport can be expected in Figure 46 and Figure 47. For that reason, the distribution of the saturation rate at x=140m is shown in Figure 50. For every time step a saturation rate is determined. Those rates are shown as a fraction. The maximum saturation is set to 1.1. So all saturation rates larger than 1.1 are equalized to 1.1. Then, it can be seen that 85% of time the transport saturated and, so, transport limited. Still 15% of the cases are not saturated. For an

increasing cross-shore position (more landward) this fraction will decrease, so, a larger fraction of the transport in time is saturated (Figure 51). That results in larger total transport for an increasing cross-shore position as can be seen in Figure 47. Supply limitation is the explanation for the increasing total transport and the decreasing small saturation fraction: If the wind velocity is not that large the transport is limited by supply and a wider beach has more available sediment.

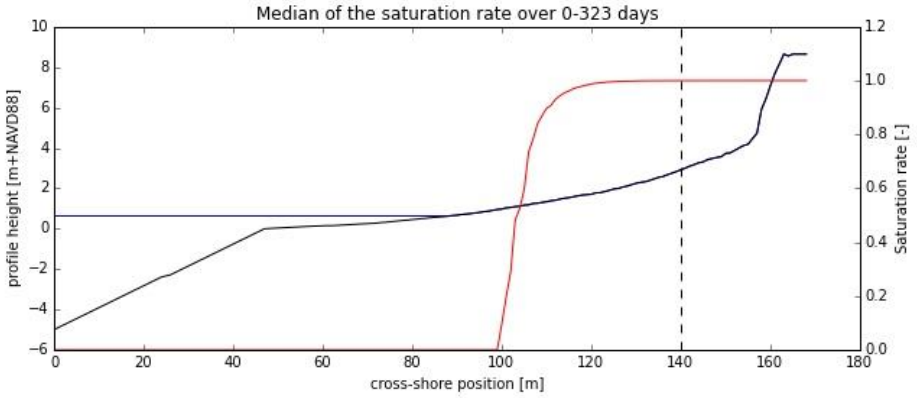

Figure 49; Median of the saturation rate

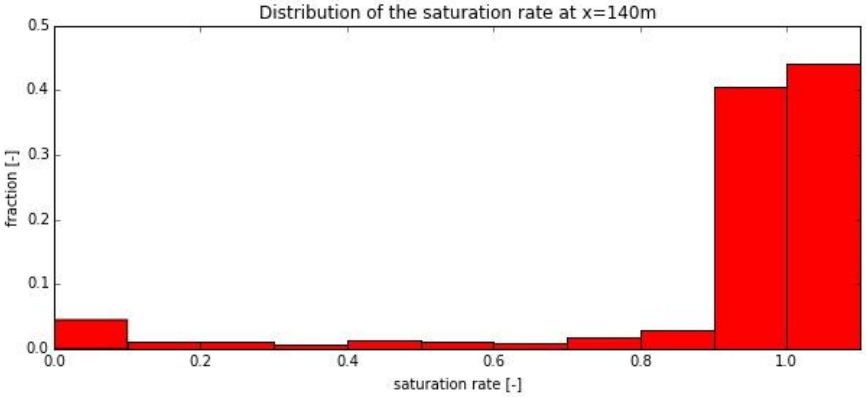

Figure 50; Distribution of the saturation rate for the sediment transport at x=140m

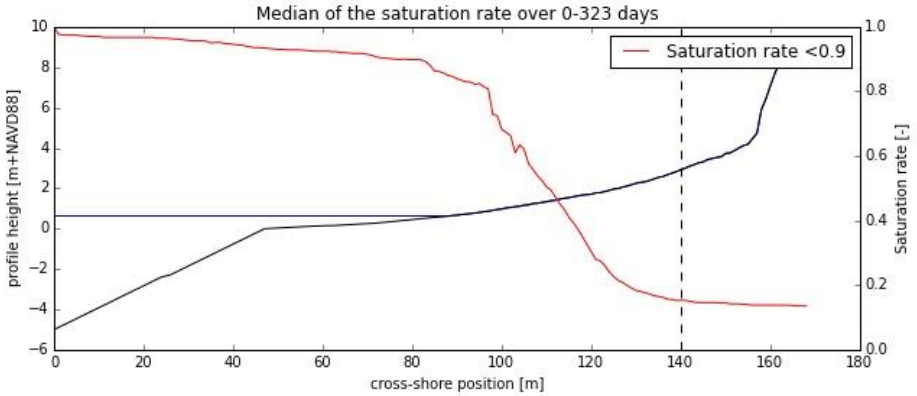

Figure 51; Saturation rate smaller than 0.9 indicated in space

The total transport into the dunes at the cross-shore position x=140m can be compared to the accretion measured in the data analysis of Chapter 3 (Table 5). Therefore, the assumption has to be made that all the

sediment that is transported into dunes, settles in the dunes. This assumption is treated in more detail in section 5.2.2. As mentioned before, offshore transport is also neglected in the model simulation. In Table 5 can be seen that both determinations are in the same range, but with the remark that in the model analysis several assumptions are made to model the Fire Island case.

Table 5; Accretion volumes Fire Island

Analysis	Data analysis	Model analysis
Volume > 3m+NAVD88 (m^3/m)	17	16.8

4.3.1 SENSITIVITY ANALYSIS

The sensitivity analysis covers the variation of the grain size distribution, because there is no such data available. The sensitivity to the grain size distribution gives more insight in the importance of measurements. Next part of sensitivity analysis is the fetch. The Fire Island results showed that the transport is supply limited and transport limited. Therefore, the beach width is part of further analysis and the adaptation time scale to investigate its effect on the supply. The adaptation time scale determines in what time the sediment transport concentration reacts to changes in the equilibrium sediment transport concentration (due to changes in wind velocity). If there is more time required to adapt, there is also more space required (see also section 2.3.2).

4.3.1.1 GRAIN SIZE DISTRIBUTION

The grain size distribution is varied in different ways to test the sensitivity of model results to initial distributions. The mean of a lognormal grain size distribution is changed in Table 6. The geometric standard deviation of the lognormal grain size distribution is changed in Table 7. The values chosen in the sensitivity analysis are based on La Selle et al. (in prep.)

Table 6; The total sediment transport rate and saturation rate at x=140m for a log normal grain size distribution with a geometric standard deviation of 2 over the accretion period

Geometric mean (µm)	400	425	450	475	500	525	550	575	600
Transport [m^3/m]	19.0	18.3	17.8	17.3	**16.8**	16.4	16.0	15.7	15.3
Relative difference to default (%)	13	9	6	3	**0**	-2	-5	-7	-9

Table 7; The total sediment transport rate and saturation rate at x=140m for a lognormal grain size distribution with a geometric mean of 500 µm over the accretion period

Log of the Geometric standard deviation	1.50	1.60	1.75	1.85	1.95	2.00	2.15	2.25
Geometric standard deviation (µm)	31.6	39.8	56.2	70.8	89.1	**100**	141.3	177.8
Transport [m^3/m]	17.4	17.3	17.0	16.9	16.8	**16.8**	16.8	16.9
Relative difference to default (%)	4	3	1	1	0	**0**	0	1

From Table 6, it can be concluded that increasing the geometric mean of the lognormal grain size distribution decreases the total transport and the saturation. The same wind velocity picks up less sediment (decreasing saturation) and has to pick relative larger sediment (increasing geometric mean). This causes a decreasing total transport.

From Table 7 it can be concluded that an increasing geometric standard deviation has little effect on the total transport. The total transport is decreasing, but it decreases at a small rate. A small geometric standard deviation represents almost no tail of the lognormal distribution. There are also less fine grains available. The smaller standard deviation outweighs the lesser amount of fine grains. It can be seen that for a standard deviation of 2.25 the amount of fines is that large that the total transport is increasing again. Figure 52 indicates two different standard deviations for the same mean grain size.

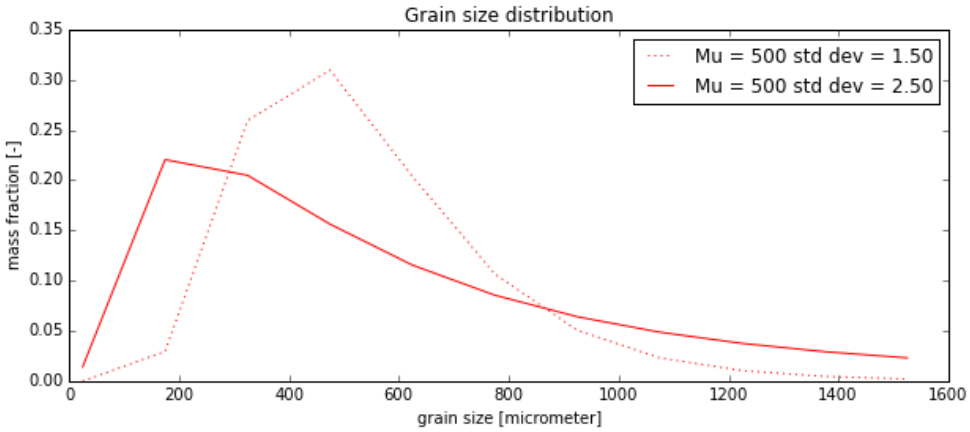

Figure 52; Grain size distribution with a mean of 500 micrometer and a geometric standard deviation of 1.50 and 2.50

4.3.1.2 FETCH

Next to the grain size distribution, the fetch is also subject to further analysis. To do this, the cross-shore position of the reference point is moved. So, it is possible to change the fetch without changing the cross-shore profile. The cross-shore positions, which are analysed in Table 8, are with reference to the position where the elevation is approximately 3.0m+NAVD88 (Figure 53). The beach width values are based on the difference beach widths determined during the data analysis, for example Figure 22.

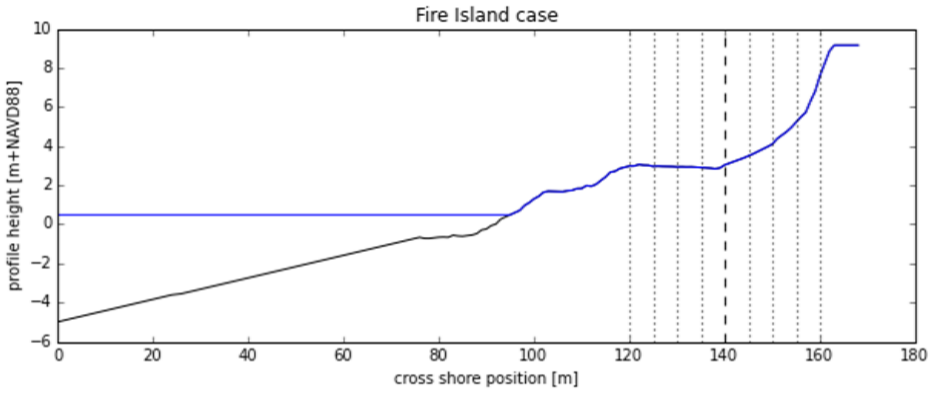

Figure 53; Overview of the sensitivity analysis of the fetch. The thick dashed line is the position where the elevation is approximately 3.0m+NAVD88. The other dashed lines are 5m or multiple from 5m away from the reference point.

Table 8; Effect of the variation of the fetch by changing the reference point on the transport rate and saturation rate. X is the position where the elevation is approximately 3.0m+NAVD88. The total transport is over the accretion period.

Δ fetch (m)	-20	-15	-10	-5	X=140m	+5	+10	+15	+ 20
Transport [m^3/m]	13.7	14.9	15.7	16.3	**16.8**	17.2	17.5	17.8	18.0
Relative difference to default (%)	-18	-11	-7	-3	**0**	2	4	6	7

From Table 8, it can be seen that, while the fetch increases, the transport rate increases as well. The transport is supply limited. A larger beach width provides more sediment to pick up. So, the source for the transport is increasing and, therefore, the total transport will increase. Both make sense in combination with the increasing saturation rates which are shown in Figure 50.

Table 9; Sensitivity of the total transport during the accretion period for the adaptation time scale

Adaptation time scale (s)	1.00	1.10	1.20	1.30	1.40	1.50	1.60	1.70	1.80	1.90	2.00
Transport [m^3/m]	**16.8**	16.7	16.5	16.3	16.1	15.9	15.7	15.5	15.2	15.0	14.8
Relative difference to default (%)	**0**	-1	-2	-3	-4	-5	-7	-8	-10	-11	-12

Table 9 shows the sensitivity of the AeoLiS model to the adaptation time scale. The sediment transport adapts asymptotically in time towards the equilibrium sediment transport capacity after a change in wind velocity. An increase of the adaptation time scale caused a decrease of the total transport as can be expected by the advection equation shown in section 2.3.2. This also indicates the effect of the fetch on the total transport and it can be seen here that the transport is depending on the adaptation time scale. Smaller values than an adaptation time scale of 1.00 s are not taken into account (de Vries et al., 2014; Davidson-Arnott et al., 2008).

4.3.2 SUMMARY

The sensitivity analysis is concluded by the comparison of the four different analyses done. This is possible by making a normalization of the total sediment transport. By comparing the different analysis, the analysis with the most impact can be determined.

Figure 54 shows the different sensitivity analyses. The red star indicates the model result that is the same in all four analyses (so called default values). The red stars are the same for every sensitivity analysis and are set to 1. As the values on the x-axis are based on literature and the data analysis, they are within the range that can be expected in reality a comparison is possible. It can be concluded that beach width affects the total transport the most, also the mean of the grain size distribution has a significant contribution. The variation of the adaptation time scale affects the total transport to a lesser extent. Variation of the standard deviation affects the total transport not very clear.

So, it can be concluded that the model is most sensitive for a variation in the beach width and the mean of the grain size distribution. Furthermore, differences in total transport due to beach width variations are caused by supply limitation. At last, it is concluded that the total transport determined by the model has an uncertainty of approximately 13% based on variations of the grain size distribution (La Selle et al. (in prep.)), other uncertainties are not quantified.

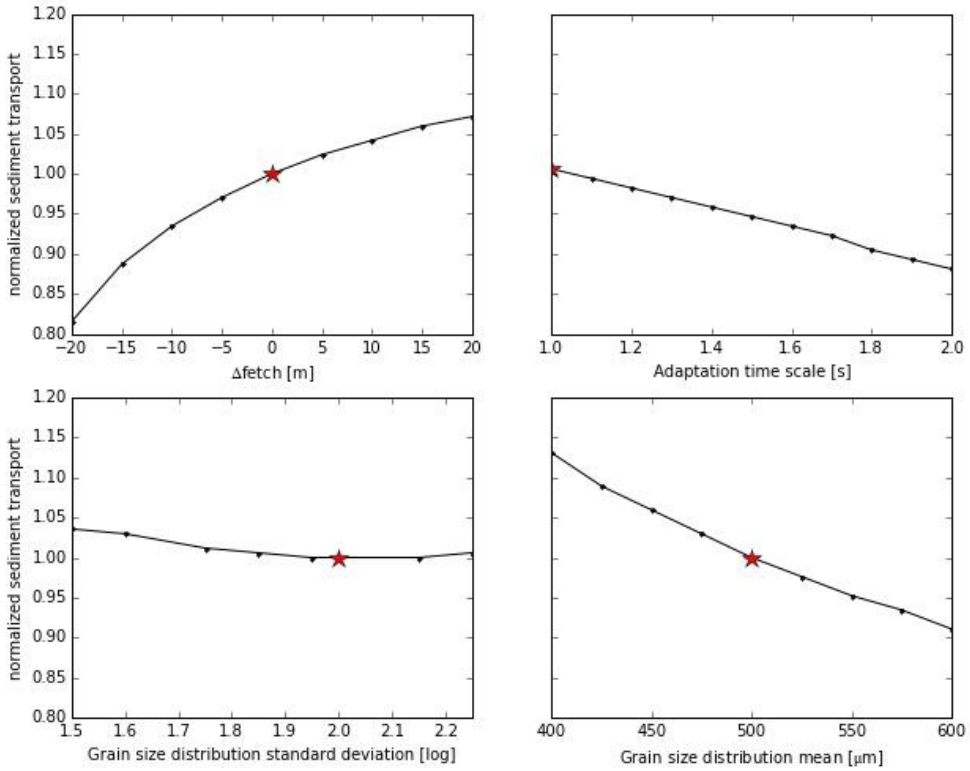

Figure 54; Normalization of the sensitivity analyses of the fetch, adaptation time scale and the mean and standard deviation of the grain size distribution

4.4 CONCLUSION

For the accretion period at Fire Island, a hindcast was done with the AeoLiS model using input from the data analysis of Chapter 3. The AeoLiS model predicted an accretion of the dunes of 16.8 m^3/m (Table 5) with an uncertainty of approximately 13% based on variations in grain size distribution (Section 4.3.1). Other uncertainties are not quantified. It is assumed that the total flux into the dunes will settle in the dunes. Comparing these results to the results from the data analysis, showed that the hindcast was in the same range. The general validity of the results depends on several assumptions. The main assumption is; the model only included onshore transport, while the wind direction was variable and mainly offshore during the accretion period.

The sensitivity analyses indicated that the model simulation of Fire Island is most sensitive for a variation in the beach width and the mean of the grain size distribution. Furthermore, it can be concluded that the aeolian sediment transport on Fire Island is often transport limited (85%) but occasionally supply limited (15%).

5 DISCUSSION

During the course of this thesis, a number of topics of interest have come up which are open for discussion. A critical reflection is made, regarding those topics of interest, relevant for this thesis. These will be presented in this chapter.

5.1 ACCURACY DATA ANALYSIS

5.1.1 PROFILE MEASUREMENTS CONDUCTED BY THE USGS

The data analysis described in Chapter 3 made use of measurements conducted by the USGS. The accuracy of those measurements was mentioned in section 3.1.1. Especially, the horizontal variability of the profile measurements is enough to introduce apparent changes in the bed elevation. Overall, there was an observed increase of the bed elevation which may be due to the recovery by aeolian sediment transport. This increase, nevertheless, could also be caused by the inaccuracy of the measurements. Besides, the profile measurements are just one measurement for one profile at a time. So, it is not possible to take a spatial average to remove the horizontal variability. The lidar data, that could give a decisive answer, is not available that frequent. However, from the lidar data it can be concluded that there was accretion in Period 1. So it was concluded that the individual profile measurements have to show accretion as well.

5.1.2 LOCAL WIND EFFECTS

The wind data did not support the beach and dune accretion as a result of the welding bar. The wind directions are mainly offshore and also the transport potential is mainly offshore. However, the wind data was measured 55 kilometers offshore. Onshore the topography of the dunes can affect the local wind directions and, therefore, the direction of the aeolian sediment transport. Lynch et al. (2009) showed in experiments that an offshore wind could result in an onshore wind direction in the zone nearshore in the lee of the dune. The wind did not change in one particular direction but separated in all different directions including onshore directed. This secondary airflow could cause foredune accretion. Lynch et al. (2013) describe, in further research, that changes in wind direction are different in time and place. They state that, for the understanding of the secondary airflow and the sediment transport, it is necessary to explain erosion or accretion in beach-dune systems. Also, Jackson et al. (2011) found reversal wind direction in the lee of the dune for offshore winds. The authors used a combination of modelling and field measurements. Results of this research indicate that wind can change from direction up to 20 meters from the dune toe and still have a significant wind velocity that makes pick up of sediment possible. The Fire Island beach is in general larger than 20 meters, on average approximately 60 meters, but it can still be considered as a hypothesis for further research.

Sea breeze is another local effect that could influence the wind direction. Sea breeze is a gentle wind as a result of heat energy that is transferred from the surface of the earth to the atmosphere (Estoque, 1961). Sea breeze can be strong enough to have its effects on coastal processes (Masselink, 1998; Sonu et al., 1973). The wind speed in a sea breeze can be as high as 10 m/s and, therefore, it can affect aeolian sediment transport as well.

The AeoLiS model is designed to receive a local wind field. The assumption was made that the wind data at the buoy is the same as at Fire Island. Local wind effects could have changed that wind data. So to improve testing against measured topographic data, local wind data is required.

5.2 AEOLIS MODEL SIMULATIONS

5.2.1 HYDRODYNAMICAL SEDIMENT TRANSPORT

The AeoLiS model used solely aeolian sediment transport processes. Hydrodynamic sediment transport was not directly part of the model. Nevertheless, hydrodynamic sediment transport and aeolian sediment transport are both important features in the intertidal zone. In the present model, the influence of the hydrodynamics is limited to mixing of the top layer of the bed. Accretion and erosion of that top layer is not included, while hydrodynamics can have significant effect in the intertidal area. Especially in case of a welding bar, those hydrodynamics are interesting. The present model imposed the welding of a bar. Not only the bathymetry can be affected by the hydrodynamics, also the grain size distribution can be affected by the hydrodynamics (van Rooijen et al., 2012 ; Reniers et al., 2013). The effect of hydrodynamics on the grain size distribution of a welding bar compared to the grain size distribution on the beach is still not well understood. This has to be subject to further research.

5.2.2 SEDIMENT TRANSPORT INTO THE DUNES

The sediment in the air is sampled from the simulations at a certain cross-shore position. The volume passing that cross-shore position is compared to the increased volume of Fire Island. So, the assumption is made that all sediment passing the cross-shore position settles in the dunes. That assumption has to be tested. The test can be done by using a more detailed coastal dune model (Kroy et al., 2002; Duran & Moore, 2013) or by making measurements of sediment transport.

So if not all the sediment settles in the dunes, the model overestimates the accretion of the dunes. Comparing the model results and the data analysis, it can be seen that the transport volume into the dunes in the model is larger than the actual settlement of sediment in the dunes. That confirms the hypothesis that the model presents an overestimation.

6 CONCLUSIONS AND RECOMMENDATIONS

6.1 CONCLUSION

The conclusions follow the research objectives as set in section 1.3:

1. ***What are the main processes and behaviour in the recovery of Fire Island?***

The analysis on Fire Island showed that, during the period 7 November 2012 until 26 September 2013 accretion occurred in the areas of interest. The accretion of the dune was 17 m^3/m (elevation above 3.0m+NAVD88 (3.0m–5.0m+NAVD88 + >5.0m+NAVD88) (Table 3)) with an uncertainty of approximately 5%. In this period the island was recovering from the impact of Hurricane Sandy. During this accretion period a welding bar was observed. This welding bar could be an important mechanism for the accretion of the areas of interest as accretion was seen in the period after the welding of the bar. The reason for this accretion could be the increasing fetch and the addition of new sediment.

Under idealized circumstances it can be assumed that the total flux settles in the dunes. The determination of the total transport under these circumstances using Bagnold's formulation indicates a larger increase (31.6 m^3/m) than is actually measured. This indicates that the actual accretion of the dunes is limited.

2. ***Is the AeoLiS model able to hindcast the recovery of Fire Island?***

The AeoLiS model predicted accretion of the dunes of 16.8 m^3/m during the period 7 November 2012 until 26 September 2013 (Table 5) with an uncertainty of approximately 13% based on variations of the grain size distribution (Section 4.3.1). Other uncertainties are not quantified. There is assumed that the total flux into the dunes settles in the dunes. Comparing these results to the results from the data analysis, showed that the hindcast was in the same range. The general validity of the results depends on several assumptions. For example, the model only included onshore transport, while the wind direction was variable and mainly offshore during the accretion period.

The sensitivity analyses indicated that the model simulation of Fire Island is most sensitive for a variation in the beach width and the mean of the grain size distribution. Furthermore, it can be concluded that the aeolian sediment transport on Fire Island is often transport limited (85%) but occasionally supply limited (15%).

3. ***What processes and data are missing for a hindcast with the AeoLiS model?***

The improvements for the AeoLiS model can be summarized as improvements to the initial conditions.

The accretion of Fire Island in the data analysis is based on lidar data. Then, the lidar data is compared to 1D transects. Those 1D transects are also imposed in the AeoLiS model. Using a 2DH bathymetry with both x-directions and y-directions could give more information about aeolian sediment transport.

The grain size distribution for Fire Island is not known in detail. The sensitivity analysis conducted in section 4.3.1 indicated that the effect of the uncertainty of the mean and standard deviation of the grain size distribution on the total transport is 13%.

6.2 RECOMMENDATIONS

This section provides the recommendations regarding the conducted research. The recommendations are separated in two parts. Firstly, recommendations are presented which are of interest for present research. Secondly, recommendations are provided to guide future model development.

Recommendations for present research are:

- *Local wind data* - Improved local wind measurements could help to improve understanding the local aeolian sediment transport beyond what was done in this thesis.

- *Increase accuracy profile measurements* - Improved accuracy of the measurements could help to indicate dune accretion from measurements inaccuracies more clearly.

- *Generalization of the results* - This model analysis was conducted at a single location. The approach could be conducted at multiple locations to determine whether the results are generally valid. The data analysis did indicate the general validation for multiple profiles.

- *Grain size measurements* - No grain size measurements were available. Measurements of the grain size distribution could help to better understand the model accuracy as was indicated in the sensitivity analysis (4.3.1.1).

Recommendations to guide future research:

- *Extend model domain* - The AeoLiS model focuses on the entrainment of sediment on the beach. Extend the domain to the dunes and include settlement of sediment in the dunes. Furthermore, the morphologic changes due to hydrodynamic sediment transport can be added by extending the model domain seawards. This can give more insight in the role of welding bars for the accretion of the dunes.

- *Morphologic changes due to aeolian and hydrodynamic sediment transport* - Morphologic changes are now imposed in the model. Including morphologic changes due to hydrodynamic and aeolian sediment transport could give more insight in the processes due to the same morphologic changes. For now, it is not well-known what those effects could be. It would be interesting to see how the morphologic changes develop due to aeolian transport.

- *Model validation for a 2D situation* - The present research focuses on a 1D understanding of the processes in the recovery of Fire Island. Validation of a 2D situation can improve that understanding.

LIST OF FIGURES

LIST OF TABLES

SYMBOLS

α	constant to convert from measured wind velocity to shear velocity	-
α_w	wind direction	°
α_{ref}	reference angle (Fire Island = 157.5)	°
ϕ	Krumbein phi scale	-
ρ_a	density of the air	kg/m^3
ρ_p	density of the grains	kg/m^3
ρ_w	density of water	kg/m^3
A	constant in formulation for wind velocity threshold based on grain size	-
C_b	empirical constant depending on the width of the grain size distribution	-
C_t	instantaneous transport concentration	kg/m^3
C_u	equilibrium transport concentration	kg/m^3
$\hat{C}_u$	equilibrium transport concentration as mass per unit area	kg/m^2
D_n	reference grain size	m
D	deposition	kg/m^2
D_p	diameter particle	mm
D_0	reference diameter of 1	mm
E	erosion	kg/m^2
S_e	available sediment in the bed	kg/m^2
T	adaptation time scale	s
T_{dry}	drying time scale	s
a	arbitrary width	m
d_n	median grain size	m
dt	time step	s
f_{uth}	factor to determine the effect of moisture on the threshold velocity	-
g	gravitational constant	m/s^2
h	saltation height	m
k	bed roughness	m
l	mean trajectory length	m
mc	moisture content	-
mg	dry mass content	-
p	porosity	-
q_{eq}	equilibrium sediment transport rate	kg/m/s
u_w	wind velocity	m/s
$u_{w,cor}$	wind velocity corrected for an angle	m/s
u_*	shear velocity	m/s
u_{*th}	shear velocity threshold	m/s
u_{th}	velocity threshold	m/s
z	height at which the wind velocity is measured	m

BIBLIOGRAPHY

Aagaard, T., Hughes, M., Møller-Sørensen, R., & Andersen, S. (2006). Hydrodynamics and Sediment Fluxes across an Onshore Migrating Intertidal Bar. *Journal of Coastal Research*, *222*(2001), 247–259. http://doi.org/10.2112/04-0214.1

Bagnold, R. (1935). The movement of desert sand. *Geographical Journal*, 342–365.

Bauer, B. O., & Davidson-Arnott, R. G. D. (2003). A general framework for modeling sediment supply to coastal dunes including wind angle, beach geometry, and fetch effects. *Geomorphology*, *49*, 89–108. http://doi.org/10.1016/S0169-555X(02)00165-4

Bauer, B. O., Davidson-Arnott, R. G. D., Hesp, P. A., Namikas, S. L., Ollerhead, J., & Walker, I. J. (2009). Aeolian sediment transport on a beach: Surface moisture, wind fetch, and mean transport. *Geomorphology*, *105*(1-2), 106–116. http://doi.org/10.1016/j.geomorph.2008.02.016

Bosboom, J., & Stive, M. J. F. (2013). *Coastal Dynamics I. Delft University of Technology. VSSD.* (0.4 ed.). Delft: VSSD.

Chris Houser, Brian Greenwood, & Troels Aagaard. (2006). Divergent response of an intertidal swash bar. *Earth Surface Processes and Landforms*, *31*, 1775–1791. http://doi.org/10.1002/esp.1365

Davidson-Arnott, R. G. D., Yanqi, Y., Ollerhead, J., Hesp, P. A., & Walker, I. J. (2008). The effects of surface moisture on aeolian sediment transport threshold and mass flux on a beach. *Earth Surface Processes and Landforms*, *33*(1), 55–74.

de Vries, S., Southgate, H. N., Kanning, W., & Ranasinghe, R. (2012). Dune behavior and aeolian transport on decadal timescales. *Coastal Engineering*, *67*, 41–53. http://doi.org/10.1016/j.coastaleng.2012.04.002

de Vries, S., van Thiel de Vries, J. S. M., van Rijn, L. C., Arens, S. M., & Ranasinghe, R. (2014). Aeolian sediment transport in supply limited situations. *Aeolian Research*, *12*, 75–85. http://doi.org/10.1016/j.aeolia.2013.11.005

Delgado-Fernandez, I. (2010). A review of the application of the fetch effect to modelling sand supply to coastal foredunes. *Aeolian Research*, *2*(2-3), 61–70. http://doi.org/10.1016/j.aeolia.2010.04.001

den Bieman, J. P. (2012). Simulating Barrier Island Evolution. *MSc. Thesis Delft University of Technology*.

Duran, O., & Moore, L. J. (2013). Vegetation controls on the maximum size of coastal dunes. *Proceedings of the National Academy of Sciences*, *110*(43), 17217–17222. http://doi.org/10.1073/pnas.1307580110

Estoque, M. A. (1961). A Theoretical Investigation of the sea breeze. *Quarterly Journal of the Royal Meteorological Society*, *87*(372), 136–146. http://doi.org/10.1002/qj.49708737203

Hapke, C. J., Lentz, E. E., Gayes, P. T., McCoy, C. a., Hehre, R., Schwab, W. C., & Williams, S. J. (2010). A Review of Sediment Budget Imbalances along Fire Island, New York: Can Nearshore Geologic Framework and Patterns of Shoreline Change Explain the Deficit? *Journal of Coastal Research*, *263*, 510–522. http://doi.org/10.2112/08-1140.1

Henderson, R.H., Hapke, C.J., Brenner, O.T., and Reynolds, B. J. (2015). *Hurricane Sandy beach response and recovery at Fire Island, New York: Shoreline and beach profile data, October 2012 to October 2014*. Retrieved from http://dx.doi.org/10.3133/ds931

Hoonhout, B. M. (2015). WindGenerator. Retrieved from http://openearth.github.io/aeolis-python/sourcecode.html#windgenerator

Hoonhout, B. M., & Vries, S. De. (2016). Process-based Modeling of Sediment Sorting and Beach Armoring and their Influence on Coastal Aeolian Sediment Transport. *In Prep.*

Houser, C. (2009). Synchronization of transport and supply in beach-dune interaction. *Progress in Physical Geography*, *33*(6), 733–746. http://doi.org/10.1177/0309133309350120

Houser, C., & Hamilton, S. (2009). Sensitivity of post-hurricance beach and dune recovery to event frequency. *Earth Surface Processes and Landforms*, *34*(5), 613–628. http://doi.org/10.1002/esp.1730

Houser, C., Wernette, P., Rentschlar, E., Jones, H., Hammond, B., & Trimble, S. (2015). Post-storm beach and dune recovery: Implications for barrier island resilience. *Geomorphology*, *234*, 54–63. http://doi.org/10.1016/j.geomorph.2014.12.044

Hsu, S. A. (1971). Wind stress criteria in eolian sand transport. *Journal of Geophysical Research*, *76*(36), 8684–8686.

Ilgar Safak; John C. Warner; Jeffrey H. List. (n.d.). Shoreface connected ridges induce formation of persistent coastline undulations. *In Prep.*

Jackson, D. W. T., Beyers, J. H. M., Lynch, K., Cooper, J. A. G., Baas, A. C. W., & Delgado-Fernandez, I. (2011). Investigation of three-dimensional wind flow behaviour over coastal dune morphology under offshore winds using computational fluid dynamics (CFD) and ultrasonic anemometry. *Earth Surface Processes and Landforms*, *36*(8), 1113–1124. http://doi.org/10.1002/esp.2139

Kathleen E. Wilson; Erika E. Lentz; Jennifer Miselis; Ilgar Safak. (n.d.). Forecasting near-term beach recovery using probabilistic networks. *In Prep.*

Kawamura, R. (1951). Study of sand movement by wind. *Tech. Rep. HEL-2-8*, Hydraulics Engineering Laboratory, Univeristy of C.

Kroy, K., Sauermann, G., & Herrmann, H. J. (2002). Minimal Model for Sand Dunes. *Physical Review Letters*, *88*(5), 054301. http://doi.org/10.1103/PhysRevLett.88.054301

La Selle, S.M., Lunghino, B.D., Jaffe, B.E., Gelfenbaum, G. (2016). Characterizing Hurricane Sandy, Washover Deposits on Fire Island, NY. *In Prep.*

Leatherman, S. (1982). *Barrier Island Handbook*. *Coastal publication series*.

Leatherman, S. P. (1985). Geomorphic and stratigraphic analysis of Fire Island, New York. *Marine Geology*, *63*, 173–195.

Lippmann, T. C., Holman, R. A., & Hathaway, K. K. (1993). Episodic, Nonstationary Behavior of a Double Bar System at Duck, North Carolina, U.S.A., 1986–1991. *Journal of Coastal Research*, (15), 49–75.

Long, J. W., Plant, N. G., Dalyander, P. S., & Thompson, D. M. (2014). A probabilistic method for constructing wave time-series at inshore locations using model scenarios. *Coastal Engineering*, *89*(February), 53–62. http://doi.org/10.1016/j.coastaleng.2014.03.008

Lynch, K., Delgado-Fernandez, I., Jackson, D. W. T., Cooper, J. A. G., Baas, A. C. W., & Beyers, J. H. M. (2013). Alongshore variation of aeolian sediment transport on a beach, under offshore winds. *Aeolian Research*, *8*, 11–18. http://doi.org/10.1016/j.aeolia.2012.10.004

Lynch, K., Jackson, D. W. T., & Cooper, J. A. G. (2009). Foredune accretion under offshore winds. *Geomorphology*, *105*(1-2), 139–146. http://doi.org/10.1016/j.geomorph.2007.12.011

Masselink, G. (1998). The effect of sea breeze on beach morphology, surf zone hydrodynamics and sediment resuspension. *Marine Geology*, *146*(1-4), 115–135. http://doi.org/10.1016/S0025-3227(97)00121-7

National Data Buoy Center. (n.d.). NDBC/NOAA wave buoy data. Retrieved from http://www.ndbc.noaa.gov/data_availability/data_avail.php

National Park Service. (2015). *2015 Tide Tables Fire Island National Seashore*. Retrieved from https://www.nps.gov/fiis/planyourvisit/upload/Tide-Tables-15-Final.pdf

Nganyi, J., Akrofi, J., Farmer, T., UNEP-GPA, WMO, & UNEP-WCMC. (2010). The ever more popular coasts. Retrieved from http://www.oceansatlas.org/servlet/CDSServlet?status=ND0xODc3JjY9ZW4mMzM9KiYzNz1rb3M~

NOAA. (n.d.). Digital Coast. Retrieved from https://coast.noaa.gov/digitalcoast/

NOAA. (2013). Tidal stations. Retrieved from https://tidesandcurrents.noaa.gov/stations.html

Owen, P. R. (1964). Saltation of uniform grains in air. *J. Fluid Mech*, *20*(2), 225–242.

Plant, N. G., & Holland, K. T. (2011a). Prediction and assimilation of surf-zone processes using a Bayesian network. Part I: Forward models. *Coastal Engineering*, *58*(1), 119–130. http://doi.org/10.1016/j.coastaleng.2010.09.003

Plant, N. G., & Holland, K. T. (2011b). Prediction and assimilation of surf-zone processes using a Bayesian network. Part II: Inverse models. *Coastal Engineering*, *58*(3), 256–266. http://doi.org/10.1016/j.coastaleng.2010.11.002

Reniers, A. J. H. M., Gallagher, E. L., MacMahan, J. H., Brown, J. A., Van Rooijen, A. A., Van Thiel De Vries, J. S. M., & Van Prooijen, B. C. (2013). Observations and modeling of steep-beach grain-size variability. *Journal of Geophysical Research: Oceans*, *118*(2), 577–591. http://doi.org/10.1029/2012JC008073

Roelvink, D., Reniers, A., van Dongeren, A., van Thiel de Vries, J., McCall, R., & Lescinski, J. (2009). Modelling storm impacts on beaches, dunes and barrier islands. *Coastal Engineering*, *56*(11-12), 1133–1152. http://doi.org/10.1016/j.coastaleng.2009.08.006

Ruz, M.-H., & Meur-Ferec, C. (2004). Influence of high water levels on aeolian sand transport: upper beach/dune evolution on a macrotidal coast, Wissant Bay, northern France. *Geomorphology*, *60*(1-2), 73–87. http://doi.org/10.1016/j.geomorph.2003.07.011

Sauermann, G., Kroy, K., & Herrmann, H. J. (2001). A Continuum Saltation Model for Sand Dunes. *Physical Review*, *64*(3). http://doi.org/10.1103/PhysRevE.64.031305

Schwab, W. C., Baldwin, W. E., Hapke, C. J., Lentz, E. E., Gayes, P. T., Denny, J. F., … Warner, J. C. (2013). Geologic Evidence for Onshore Sediment Transport from the Inner Continental Shelf: Fire Island, New York. *Journal of Coastal Research*, *29*(2011), 526–544. http://doi.org/10.2112/jcoastres-d-12-00160.1

Sonu, C. J., Murray, S. P. ., Hsu, S. A., Suhayda, J. N., & Waddel, E. (1973). Sea breeze and coastal processes. *EOS*, *54*(9), 820–833. http://doi.org/10.1029/EO054i009p00820

Stive, M. J. F., Schipper, M. A. de, Luijendijk, A. P., Aarninkhof, S. G. J., Gelder-Maas, C. van, Vries, J. S. M. van T. de, … Ranasinghe, R. (2013). The Sand Engine : A solution for the Dutch Delta in the 21 st C entury ? *Journal of Coastal Research*, *29*(5), 1001–1008.

Stockdon, H. F., Holman, R. A., Howd, P. A., & Sallenger, A. H. (2006). Empirical parameterization of setup, swash, and runup. *Coastal Engineering*, *53*(7), 573–588. http://doi.org/10.1016/j.coastaleng.2005.12.005

USGS. (2016). Fire Island Coastal Change research. Retrieved from http://coastal.er.usgs.gov/fire-island/

van Rooijen, A., Reniers, A., van Thiel de Vries, J., Blenkinsopp, C., & Mccall, R. (2012). Modelling swash zone sediment transport at Le Truc Vert, France. In *Coastel Engineering Proceedings* (pp. 1–12).

Walstra, D. J. R., Reniers, A. J. H. M., Ranasinghe, R., Roelvink, J. A., & Ruessink, B. G. (2012). On bar growth and decay during interannual net offshore migration. *Coastal Engineering*, *60*(1), 190–200. http://doi.org/10.1016/j.coastaleng.2011.10.002

Wikipedia. (2016). Monte Carlo Markov Chain. Retrieved from https://en.wikipedia.org/wiki/Markov_chain_Monte_Carlo

APPENDIX A DATA ANALYSIS – VOLUME CHANGES

This appendix is a complement on the data analysis as described in section 3.2.2. Table 10 shows all the volume changes for the different profiles. The volumes changes are divided in threshold levels and periods. The periods start and stop with a lidar data set.

Table 10; Volume changes for the profiles of interest during the periods set by the lidar data

Profile		7	22	25	26	28	29	30	31
Threshold 0.0m-1.5m [m^3/m]									
07-Nov-12	**26-Sep-13**	72	-12	45	-29	-6	54	53	81
26-Sep-13	**06-Apr-14**	22	-40	-106	-16	-52	-36	-58	-72
06-Apr-14	**12-Apr-14**	-54	-7	-41	-35	-20	-20	-35	-111
Threshold 1.5m-3.0m [m^3/m]									
07-Nov-12	**26-Sep-13**	25	28	42	41	16	34	22	38
26-Sep-13	**06-Apr-14**	0	-25	-18	-40	-24	-21	-32	-28
06-Apr-14	**12-Apr-14**	-3	-16	-5	-15	-8	-5	-9	-4
Threshold 3.0m-5.0m [m^3/m]									
07-Nov-12	**26-Sep-13**	3	8	12	13	7	9	8	1
26-Sep-13	**06-Apr-14**	3	-1	0	-7	-4	-5	-5	0
06-Apr-14	**12-Apr-14**	-1	-10	-3	-7	-4	-2	-1	0
Threshold >5.0m [m^3/m]									
07-Nov-12	**26-Sep-13**	0	2	-1	4	10	1	1	0
26-Sep-13	**06-Apr-14**	0	-2	1	-1	-6	-1	0	0
06-Apr-14	**12-Apr-14**	0	-3	0	-3	-1	0	0	0
Total Change [m^3/m]									
07-Nov-12	**26-Sep-13**	100	25	98	30	27	99	83	120
26-Sep-13	**06-Apr-14**	25	-68	-123	-64	-86	-64	-95	-101
06-Apr-14	**12-Apr-14**	-58	-36	-49	-61	-33	-27	-45	-115

APPENDIX B AEOLIS MODEL CONFIGURATION

Model revision: SHA-1: a993f3ad6d1b9e1a5fb1d8e087e6004ea381ebba

```
%%%%%%%%%%%%%%%%%%%%%%%%%%%%%%%%%%%%%%%%%%%%%%%%%%%%%%%%%%%%%%%%%%%%%
%%%%%%%
%% AeoLiS model configuration                                       %%
%% Date: 2016-07-07 09:47:21                                        %%
%%%%%%%%%%%%%%%%%%%%%%%%%%%%%%%%%%%%%%%%%%%%%%%%%%%%%%%%%%%%%%%%%%%%%
%%%%%%%

A = 0.085000
CFL = 1.00
Cb = 1.50
T = 5
Tdry = 3600
Tsalt = 2592000.00
accfac = 1.00
bed_file = z.txt
bedcomp_file =
bedupdate = F
beta = 100.00
bi = 0.000000
boundary_lateral = circular
boundary_offshore = noflux
boundary_onshore = gradient
callback =
cpair = 0.001004
csalt = 0.035000
dt = 600.00
dx = 1.00
dy = 1.00
eps = 0.001000
evaporation = T
facDOD = 0.100000
g = 9.81
gamma = 0.500000
grain_dist = 0.000318 0.164250 0.229567 0.190012 0.137493 0.095622 0.065990 0.045754 0.032034 0.022691
0.016269
grain_size = 0.000025 0.000175 0.000325 0.000475 0.000625 0.000775 0.000925 0.001075 0.001225 0.001375
0.001525
gusts = F
k = 0.010000
layer_thickness = 0.005000
m = 0.500000
mask_file =
max_error = 0.000001
max_iter = 1000
meteo_file =
method_moist = belly_johnson
method_transport = bagnold
minfrac = 0.000100
mixtoplayer = T
nfractions = 11
nlayers = 5
nx = 2500
```

ny = 0
output_file = aeolis_tide1_wind0_bar0.nc
output_times = 3600.00
output_types =
output_vars = zb zs Ct Cu Ct.avg Cu.avg Ct.sum uw udir uth mass pickup w qs qn qs.sum qn.sum
phi = 40.00
porosity = 0.400000
restart =
rhoa = 1.25
rhom = 1650.00
rhop = 2650.00
rhow = 1025.00
scheme = euler_backward
sigma = 4.20
sweeptoplayer = T
th_bedslope = F
th_grainsize = T
th_humidity = F
th_moisture = T
th_roughness = F
th_salt = F
tide_file = symtide.txt
tout = 1209601
tstart = 0
tstop = 3600000
uth = 4.00
w = 0.030000
wave_file = wave.txt
wind_file = conwind.txt
xgrid_file = x.txt
ygrid_file = y.txt
z = 5.00